Defence Research and Development Canada
Recherche et développement pour la défense Canada

DEFENCE R&D DÉFENSE

The application of track before detect techniques against maritime surface targets

Michael McDonald and Bhashyam Balaji

Defence R&D Canada – Ottawa

Canada

Technical Report
DRDC Ottawa TR 2009-246
February 2010

The application of track before detect techniques against maritime surface targets

Michael McDonald
Defence R&D Canada – Ottawa

Bhashyam Balaji
Defence R&D Canada – Ottawa

Defence R&D Canada – Ottawa
Technical Report
DRDC Ottawa TR 2009-246
February 2010

Principal Author

Original signed by Michael McDonald

Michael McDonald

Approved by

Original signed by Anthony Damini

Anthony Damini
Head/Radar System

Approved for release by

Original signed by Brian Eatock

Brian Eatock
Chair/Document Review Panel

Abstract

Real radar data containing a small manoeuvring boat in sea clutter was processed using a grid based finite difference implementation of continuous-discrete filtering. An examination was undertaken to determine the appropriate dynamic, target amplitude and clutter amplitude models which should be utilized to allow the successful application of Track Before Detect techniques (TkBD). Both two dimensional diffusion and four dimensional constant velocity models were implemented using Gaussian and Rayleigh sea clutter models. Superior performance was observed for the constant velocity model and significant sensitivity was noted due to mismatches between actual clutter characteristics and Gaussian and Rayleigh models. TkBD performance was examined assuming a Rayleigh sea clutter model with embedded Swerling 0, 1 or 3 target signal models. The Swerling 0 model was observed to exhibit a heightened sensitivity to changes in measured signal strength and provided improved detection of the maritime target examined in comparison with Swerling 1 and 3 targets at the cost of more peaked or multi-modal posterior density. The potential for achieving significant detection performance improvements by utilizing K and KA distributed clutter models in place of the simpler Rayleigh distribution was demonstrated through analysis of simulated data representing spiky sea clutter. However, additional analysis using real data revealed that use of a probability distribution function more closely matched to the observed real sea clutter returns does not necessarily result in improved performance. For the data set examined, significantly degraded performance was observed when K and KA based processing is used in place of a Rayleigh based processor utilizing a simple likelihood limiting step to compensate for model mismatches due to sea clutter spikes.

Résumé

Un filtre continu discret mis en oeuvre à l'aide d'un algorithme de différences finies à grille a été utilisé pour traiter des données radar réelles comportant une petite embarcation effectuant des manoeuvres sur un fond de clutter de mer. Un examen a été effectué pour déterminer quels modèles de comportement dynamique, d'amplitude de cible et d'amplitude de clutter doivent être utilisés pour permettre d'utiliser avec succès les techniques de poursuite avant détection (TkBD). Un modèle de diffusion à deux dimensions et un modèle à vitesse constante à quatre dimensions ont été mis en oeuvre en utilisant des modèles de clutter de mer de Gauss et de Rayleigh. Le modèle à vitesse constante a offert un meilleur rendement. Ce modèle a été fort sensible aux divergences entre les caractéristiques réelles du clutter et les modèles de Gauss et de Rayleigh. Le rendement de TkBD a été étudié en supposant un modèle de clutter de mer de Rayleigh avec un modèle de signal de cible de Swerling 0, 1 ou 3 intégré. Le modèle de Swerling 0 nous a permis d'obtenir une plus grande sensibilité aux variations d'intensité du signal mesuré et de mieux détecter la cible maritime étudiée par rapport aux modèles de Swerling 1 et 3 ; cependant il a comporté l'inconvénient d'avoir une densité a posteriori comportant plus de pics et de modes. Une analyse de données

simulées représentant un clutter de mer comportant des pics a permis de démontrer qu'il était possible d'améliorer grandement le rendement de détection en utilisant des modèles de distribution du clutter K et KA. Toutefois, des analyses supplémentaires menées à l'aide de données réelles ont révélé que l'utilisation de fonctions de distribution qui correspondent mieux au comportement réel du clutter de mer ne permet pas nécessairement d'améliorer le rendement. Pour l'ensemble de données étudié, le rendement observé décroît fortement lorsqu'on utilise un traitement fondé sur des modèles K et KA plutôt qu'un traitement fondé sur le modèle de Rayleigh comportant une simple étape de limite de vraisemblance servant à compenser les divergences du modèle créées par les pics du clutter de mer.

Executive summary

The application of track before detect techniques against maritime surface targets

Michael McDonald, Bhashyam Balaji; DRDC Ottawa TR 2009-246; Defence R&D Canada – Ottawa; February 2010.

Introduction

This report summarizes the results of a multistage study to examine the application of Track Before Detect (TkBD) techniques to the detection of low radar cross-section, highly manoeuvrable, high speed maritime targets. Conventional maritime surveillance approaches adopt a multi-phase strategy in which target detections are fed to a Kalman filter based tracker. For targets, such as manoeuvring speedboats, the approach provides poor performance due to the failure of the target dynamics to meet the constant velocity requirements. In addition, target signal information is lost as a hard detection decision must be made prior to tracking via a Kalman filter. This information loss is particularly detrimental for these targets possessing very low Signal to Interference Ratios (SIR). In this report we utilize a grid-based Finite Difference (FD) algorithm which utilizes the complete measurement set from each scan to evolve the full state density probability. For the radar surveillance the measurement at each time step corresponds to radar echo returns from all range-azimuth bins within a scanned sector.

Results

An examination of TkBD techniques was undertaken against real maritime radar surveillance data to determine the appropriate dynamic, target amplitude and clutter amplitude models that must be employed to achieve useful performance. Two-dimensional diffusion and four-dimensional constant velocity models were implemented and superior performance was observed for the constant velocity model. TkBD performance was also examined assuming a Rayleigh sea clutter model with embedded Swerling 0, 1 or 3 target signal models. The Swerling 0 model is observed to exhibit a heightened sensitivity to changes in measured signal strength and provides improved detection of the maritime target examined in comparison with Swerling 1 and 3 targets at the cost of more peaked or multi-modal posterior density. The potential for achieving significant detection performance improvements by utilizing K and KA distributed clutter models was demonstrated through analysis of simulated data representing spiky sea clutter. However, additional analysis using real data reveals that the use of these probability distribution functions (PDF), which are closely matched to the observed real sea clutter amplitude histograms, does not necessarily result in improved performance. For the real data set, significant performance degration is observed when K and KA based processing is used. This is a result of the additional spatial correlation which is present in the real sea clutter returns but which is not captured by a simple PDF model.

Significance

The solution of the TkBD problem has been previously studied in the context of SAR [1], and IR [2] images. However, the targets in those studies were against simulated targets. The work in this report highlights the difficulties arising from the application of the TkBD techniques to real maritime surveillance data containing sea clutter and a manoeuvring speedboat. The results highlight the complexity of the clutter environment and the choice of stochastic model to represent it. Additional techniques, ah hoc or otherwise, must also be utilized to deal with the inevitable departures of real world signal from adopted models so as to prevent catastrophic breakdown in detection performance. The results in this report demonstrate that significant detection performance improvements can be achieved if these issues are considered and addressed.

Future Plans

The investigations undertaken in this report has resulted in spin off research on alternate models of sea clutter which allow more realistic simulation and characterization of the localized but spatially structured clutter events that exist in a typical range-azimuth scan. This research is continuing with the goal of developing more efficient detection strategies based on the parameter based identification of clutter versus target events [3].

Sommaire

The application of track before detect techniques against maritime surface targets

Michael McDonald, Bhashyam Balaji ; DRDC Ottawa TR 2009-246 ; R & D pour la défense Canada – Ottawa ; février 2010.

Introduction

Le présent rapport résume les résultats d'une étude en plusieurs étapes portant sur l'application de techniques de poursuite avant détection (TkDB) pour détecter des cibles maritimes hautes vitesses et très manoeuvrables ayant une faible surface équivalente radar. Les approches de surveillance maritime classique adoptent une stratégie à phases multiples : les détections de cibles sont envoyées à un système de poursuite à filtre de Kalman. Pour certaines cibles, comme des embarcations rapides qui effectuent des manoeuvres, cette approche n'a pas un bon rendement, car le comportement dynamique de la cible ne correspond pas aux exigences de vitesse constante. De plus, de l'information sur le signal de la cible est perdue, car il faut prendre une décision de détection ferme avant d'utiliser un filtre de Kalman pour la poursuite. Cette perte d'information est particulièrement désavantageuse pour les cibles dont le rapport signal/brouillage est très faible. Dans le présent rapport, nous utilisons un algorithme de différences finies à grille qui fait appel à l'ensemble des mesures de chaque balayage pour modifier la densité de probabilité de toutes les variables d'état. Pour la surveillance radar, la mesure à chaque intervalle de temps correspond aux échos radars pour toutes les cellules distance-azimut dans le secteur balayé.

Résultats

Une étude des techniques de poursuite avant détection a été entreprise au moyen de données réelles de radar de surveillance maritime afin de déterminer quels modèles de comportement dynamique, d'amplitude de cible et d'amplitude de clutter doivent être utilisés pour obtenir un rendement utile. Un modèle de diffusion à deux dimensions et un modèle à vitesse constante à quatre dimensions ont été mis en oeuvre ; le rendement du modèle à vitesse constante s'est avéré supérieur. Le rendement de la poursuite avant détection a également été étudié en supposant un modèle de clutter de mer de Rayleigh avec un modèle de signal cible de Swerling 0, 1 ou 3 intégré. Le modèle de Swerling 0 permet d'obtenir une plus grande sensibilité aux variations d'intensité du signal mesuré et de mieux détecter la cible maritime étudiée par rapport aux modèles de Swerling 1 et 3 ; il comporte cependant l'inconvénient d'avoir une densité a posteriori comportant plus de pics et de modes. Une analyse de données simulées représentant un clutter de mer comportant des pics a permis de démontrer qu'il était possible d'améliorer grandement le rendement de détection en utilisant des modèles de distribution du clutter K et KA. Toutefois, des analyses supplémentaires menées à l'aide de

données réelles ont révélé que l'utilisation de ces fonctions de distribution de probabilité, qui correspondent pourtant bien aux histogrammes d'amplitude mesurée du clutter de mer réel, ne permet pas nécessairement d'améliorer le rendement. Pour l'ensemble de données réelles, l'utilisation de fonctions K et KA pour le traitement dégrade le rendement de façon importante. Ce phénomène est dû à la corrélation spatiale présente dans le clutter de mer réel, corrélation qui n'est pas reproduite par un simple modèle à fonction de distribution de probabilité.

Portée

La solution au problème de TkBD a déjà été étudiée dans le contexte du radar à synthèse d'ouverture (SAR) et des images infrarouges (IR). Cependant, ces études n'ont porté que sur des cibles simulées. Les travaux faisant l'objet du présent rapport font ressortir les difficultés que présente l'application de techniques de TkBD à des données réelles de surveillance maritime qui contiennent du clutter de mer et une embarcation rapide effectuant des manoeuvres. Les résultats mettent en évidence la complexité de l'environnement de clutter et du choix du modèle stochastique à utiliser pour le représenter. Des techniques additionnelles, ad hoc ou autres, doivent être utilisées pour compenser les divergences inévitables entre les signaux réels et les modèles adoptés afin d'éviter les chutes catastrophiques du rendement de détection. Les résultats du présent rapport démontrent qu'il est possible d'améliorer fortement le rendement de détection si ces problèmes sont étudiés et résolus.

Recherches futures

Les recherches décrites dans le présent rapport ont ouvert une nouvelle voie de recherche portant sur d'autres modèles du clutter de mer. Ces nouveaux modèles permettront de simuler et de caractériser avec plus de réalisme les événements de clutter localisés, mais structurés spatialement, que l'on rencontre habituellement dans un balayage distance-azimut. Ces recherches se poursuivent en vue de la mise au point de stratégies de détection plus efficaces fondées sur la distinction des événements de clutter et des cibles selon des paramètres.

Table of contents

List of figures

This page intentionally left blank.

1 Introduction

The conventional approaches to detecting and tracking maritime targets typically adopt a multi-phase strategy in which target detections are fed to a Kalman filter based tracker. This is commonly combined with a simple linear Track Before Detect (TkBD) scheme to provide noncoherent integration prior to the final detection step. For highly manoeuvrable targets the above approach provides poor performance due to the failure of the target dynamics to meet the constant velocity requirements. In addition, the methodology fails to utilize all available target signal information since a "hard" detection decision must be made prior to tracking via a Kalman filter. This information loss is particularly detrimental for targets possessing very low Signal to Interference Ratios (SIR).

Two approaches which are commonly used for solving nonlinear continuous-discrete problems with non-analytical measurement functions are Particle Filters (PF) and grid-based methods (see, for example [4], [5]). In this study we focus on a grid-based approach and in particular, a Finite Difference (FD) algorithm. Unlike simple TkBD methods, the FD approach utilises the complete measurement set from each scan to evolve the state conditional probability density. For radar surveillance, the 'measurement' at each time step corresponds to the filtered amplitude radar echoes (or returns) from all range-azimuth bins within a scanned sector.

The solution of the TkBD problem based on the continuous-discrete filtering and continuous-continuous filtering (based on the Duncan-Mortensen-Zakai equation) has previously been studied in the context of SAR [1], and IR [2] images, or ground moving target indicator (GMTI) radar measurements [6]. However, these studies utilized simulated targets and/or simulated clutter.

This page intentionally left blank.

2 Theory

2.1 Continuous Discrete Filtering

In continuous-discrete filtering theory (see, for example, [5]), the state model is given by the Itô stochastic differential equation of the form

$$d\mathbf{x}(t) = f(\mathbf{x}(t), t)dt + e(\mathbf{x}(t), t)d\mathbf{v}(t). \tag{1}$$

Here $\mathbf{x}(t)$ is a $\mathbb{R}^n-$valued process, $f(\mathbf{x}(t), t) \in \mathbb{R}^n$, $e(\mathbf{x}(t), t) \in \mathbb{R}^{n\times p}$ and $\mathbf{v}$ is a $\mathbb{R}^p-$valued Brownian process with covariance $Q(t)$. The forward diffusion operator, $\mathscr{L}$, of the state process generated by Equation 1 is given by

$$\mathscr{L}(\cdot) = -\sum_{i=1}^{n} \frac{\partial(\cdot f_i)}{\partial x_i} + \frac{1}{2}\sum_{i,j=1}^{n} \frac{\partial^2 \left[\cdot(eQe^T)_{ij}\right]}{\partial x_i \partial x_j}. \tag{2}$$

The general continuous-discrete filtering problem considers the following signal and measurement processes:

$$\begin{cases} d\mathbf{x}(t) = f(\mathbf{x}(t), t)dt + e(\mathbf{x}(t), t)d\mathbf{v}(t), \\ \mathbf{y}(t_k) = h(\mathbf{x}(t_k), t_k, \mathbf{w}(t_k)). \end{cases} \tag{3}$$

Here $\mathbf{y}$ is a $\mathbb{R}^m-$valued process, $h(\mathbf{x}(t), t, \mathbf{w}(t)) \in \mathbb{R}^m$, and $\mathbf{w}$ is a $\mathbb{R}^q-$valued Brownian process.

The continuous-discrete filtering problem is solved as follows. Let the initial distribution be $\sigma_0(x)$ and let the measurements be collected at time instants $t_1, t_2, \ldots, t_k, \ldots$. We use the notation $Y(\tau) = \{y(t_l) : t_0 < t_l \leq \tau\}$. At observation time t_k, the conditional density is then given by

$$p(t_k, x|Y(t_k)) = \frac{p(y(t_k)|x)p(t_k, x|Y(t_{k-1}))}{\int p(y(t_k)|\xi)p(t_k, \xi|Y(t_{k-1}))\{d^n\xi\}}, \tag{4}$$

and $p(t_k, x|Y(t_{k-1}))$ is given by the solution of the Fokker-Planck-Kolmogorov forward equation (FPKfe)

$$\frac{\partial}{\partial t}p(t, x|Y(t_{k-1})) = \mathscr{L}(p(t, x|Y(t_{k-1}))), \quad t_{k-1} \leq t < t_k, \tag{5}$$

with initial condition $p(t_{k-1}, x|Y(t_{k-1}))$.

Often, the signal and measurement model is described by the following system:

$$\begin{cases} d\mathbf{x}(t) = f(\mathbf{x}(t), t)dt + e(\mathbf{x}(t), t)d\mathbf{v}(t), \\ \mathbf{y}(t_k) = h(\mathbf{x}(t_k), t_k)dt + d\mathbf{w}(t_k), \quad k = 1, 2, \ldots, \end{cases} \tag{6}$$

where $\mathbf{y}(t) \in \mathbb{R}^{m\times 1}$, $h \in \mathbb{R}^{m\times 1}$ and the noise process is described by $\mathbf{w}(t) \sim N(0, R(t))$. Then, $p(y(t_k)|x)$ is given by

$$\begin{aligned} p(y(t_k)|x) = & \frac{1}{((2\pi)^m \det R(t_k))^{1/2}} \\ & \times \exp\Big\{ -\frac{1}{2}(y(t_k) - h(x(t_k), t_k))^T \\ & \quad \times (R(t_k))^{-1}(y(t_k) - h(x(t_k), t_k))\Big\}. \end{aligned} \tag{7}$$

2.2 Dynamic Model

The simplest model to consider for the motion on a plane is the two-dimensional diffusion model. The state model is two dimensional:

$$\begin{bmatrix} d\mathbf{x}_1(t) \\ d\mathbf{x}_2(t) \end{bmatrix} = \begin{bmatrix} \sigma_1 & 0 \\ 0 & \sigma_2 \end{bmatrix} \begin{bmatrix} d\mathbf{v}_1(t) \\ d\mathbf{v}_2(t) \end{bmatrix}, \tag{8}$$

and $Q(t) = 1$. The FPKfe for the diffusion model is

$$\frac{\partial u}{\partial t}(t, x) = \left(\frac{\sigma_1^2}{2} \frac{\partial^2}{\partial x_1^2} + \frac{\sigma_2^2}{2} \frac{\partial^2}{\partial x_2^2} \right) u(t, x). \tag{9}$$

The other state model considered in this report is the constant velocity model on the plane. The resulting state model is four dimensional. If

$$\begin{bmatrix} \mathbf{x}_1(t) & \mathbf{x}_2(t) & \mathbf{x}_3(t) & \mathbf{x}_4(t) \end{bmatrix} = \begin{bmatrix} x(t) & v_x(t) & y(t) & v_y(t) \end{bmatrix}, \tag{10}$$

then the model is

$$\begin{bmatrix} d\mathbf{x}_1(t) \\ d\mathbf{x}_2(t) \\ d\mathbf{x}_3(t) \\ d\mathbf{x}_4(t) \end{bmatrix} = \begin{bmatrix} 0 & 1 & 0 & 0 \\ 0 & 0 & 0 & 0 \\ 0 & 0 & 0 & 1 \\ 0 & 0 & 0 & 0 \end{bmatrix} \begin{bmatrix} \mathbf{x}_1(t) \\ \mathbf{x}_2(t) \\ \mathbf{x}_3(t) \\ \mathbf{x}_4(t) \end{bmatrix} + \begin{bmatrix} 0 & 0 \\ 1 & 0 \\ 0 & 0 \\ 0 & 1 \end{bmatrix} \begin{bmatrix} \sigma_2 d\mathbf{v}_2(t) \\ \sigma_4 d\mathbf{v}_4(t) \end{bmatrix}. \tag{11}$$

The FPKfe for the Constant Velocity (CV) model (again, $Q(t) = 1$) is

$$\frac{\partial u}{\partial t}(t, x) = \left(\frac{\sigma_2^2}{2} \frac{\partial^2}{\partial x_2^2} + \frac{\sigma_4^2}{2} \frac{\partial^2}{\sigma x_4^2} - x_2 \frac{\partial}{\partial x_1} - x_4 \frac{\partial}{\partial x_3} \right) u(t, x). \tag{12}$$

The diffusion model should be adequate for tracking slow-movers, and the CV model is expected to be required for tracking fast movers. Since it is low-dimensional, the diffusion model can also be solved more accurately and quickly than the CV model.

The measurement model is specified by $p(y(t_k)|x)$, where a measurement $y(t_k)$ is the return amplitude on a grid.

2.3 Multiplicative Operator Splitting

The solution of the continuous-discrete filtering problem thus requires the solution of a Partial Differential Equation (PDE) of the following form:

$$\frac{\partial u}{\partial t}(t,x) = \sum_{i=1}^{s} \mathscr{L}_i u(t,x). \tag{13}$$

For the $s = 2$ diffusion model

$$\begin{aligned} \mathscr{L}_1 &= \frac{\sigma_1^2}{2}\frac{\partial^2}{\partial x_1^2}, \\ \mathscr{L}_2 &= \frac{\sigma_2^2}{2}\frac{\partial^2}{\partial x_2^2}, \end{aligned} \tag{14}$$

and for the $s = 4$ CV model we have

$$\begin{aligned} \mathscr{L}_1 &= \frac{\sigma_2^2}{2}\frac{\partial^2}{\partial x_2^2}, \\ \mathscr{L}_2 &= \frac{\sigma_4^2}{2}\frac{\partial^2}{\partial x_4^2}, \\ \mathscr{L}_3 &= -x_2\frac{\partial}{\partial x_1}, \\ \mathscr{L}_4 &= -x_4\frac{\partial}{\partial x_3}. \end{aligned} \tag{15}$$

In the Forward Euler explicit scheme (see, for instance, [7]), Equation 13 is numerically solved using the following approximation:

$$\frac{u(t+\Delta t,x) - u(t,x)}{\Delta t} = \sum_{i=1}^{s} \mathscr{L}_i u(t,x), \tag{16}$$

so that

$$\begin{aligned} u(t+\Delta t,x) &= \left(1 + \Delta t \sum_{i=1}^{s} \mathscr{L}_i\right) u(t,x), \\ &\approx \prod_{i=1}^{s} \left(1 + \Delta t \mathscr{L}_i\right) u(t,x) + O(\Delta t)^2. \end{aligned} \tag{17}$$

Note that if the time step is too large, the explicit scheme is unstable. This problem is evaded by splitting up the time interval between measurements into N_T time steps prior to applying the Forward Euler scheme, i.e.,

$$\left(1 + \Delta t \mathscr{L}_i\right) \approx \left(1 + \frac{\Delta t}{N_T}\mathscr{L}_i\right)^{N_T}. \tag{18}$$

Furthermore, stability of the discretization of the convection operators requires that "upwind differencing" be used for the first order derivative operator [7]. This also ensures that the probability remains positive.

In the Backward Euler (or Laasonen) implicit scheme, the following approximation is made:

$$\frac{u(t+\Delta t,x)-u(t,x)}{\Delta t}=\Delta t\sum_{i=1}^{s}\mathscr{L}_i u(t+\Delta t,x), \tag{19}$$

or

$$u(t+\Delta t,x)=\prod_{i=1}^{s}\left(1-\Delta t\mathscr{L}_i\right)^{-1}u(t,x). \tag{20}$$

Since the matrices are tridiagonal, the inverses may be computed efficiently using the Thomas tridiagonal method [8]. This implies that the differentiation matrices are sparse. A sparse representation leads to considerably less memory requirements and increased computational speed (due to far fewer flops). Finally, the Dirichlet boundary conditions are applied.

3 Data Description

The data used in this study were collected using the DRDC Ottawa X-band Wideband Experimental Airborne Radar (XWEAR) near the mouth of Halifax harbour in Nova Scotia, Canada. For the trial, a small highly manoeuvrable speedboat was fielded, see Figure 1. Relevant radar and aircraft operating parameters are given in Table 1.

Figure 1: *Speedboat used as target in trials.*

The raw returns were pulse compressed, then pre-processed to remove large scale fluctuations in underlying power levels. This normalization was accomplished via the well-known Cell Averaging (CA) approach in which the power in each measured range-azimuth bin is divided by the average power of the surrounding cells (see, for instance [9]). In particular, the mean power was calculated using 128 range bins from each side of the Cell Under Test (CUT) with a guard band of 30 cells between the CUT and the beginning of each averaging band to prevent self-nulling of the target signal via target contamination of the mean.

Radar Resolution	< 1 meter
Radar Scan Rate	36^o/s
Sector Width	100^o
Pulse Repetition Frequency (PRF)	500 Hz
Aircraft Altitude	1000 feet

Table 1: *Radar and Aircraft Operating Parameters*

Figure 2 presents a histogram of the measured clutter returns for the data set and the corresponding Rayleigh and Gaussian probability distribution functions (PDF) matched to the mean power and/or variance of the real data. It is readily evident that neither distribution is a particularly good match to the real data which exhibits a much longer tail corresponding

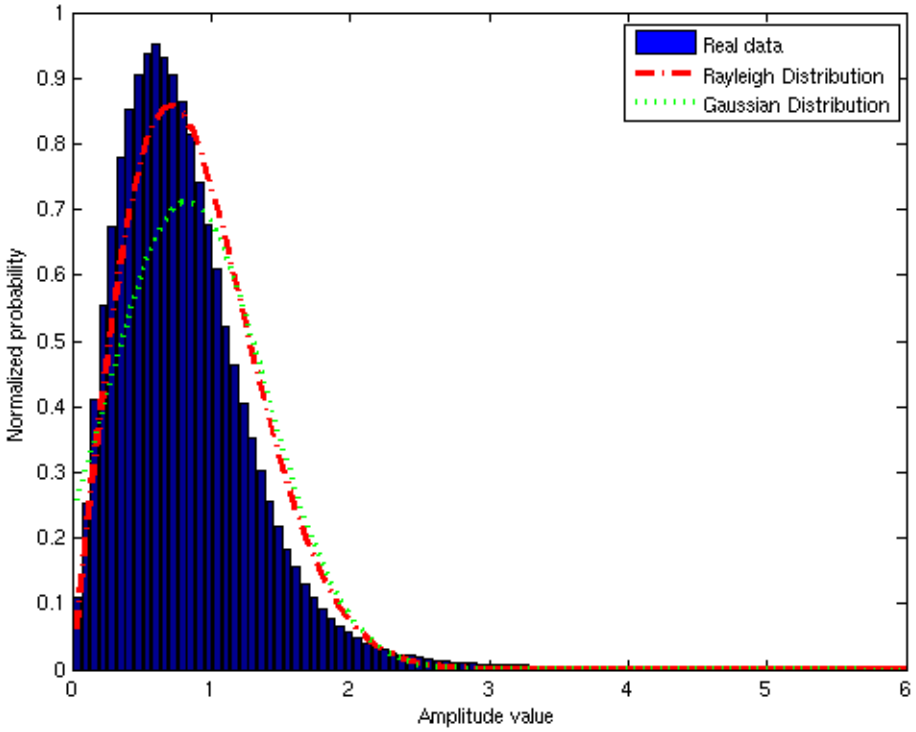

Figure 2: *Histogram of real data distribution and plots of Rayleigh and Gaussian probability distribution functions with variance and/or mean matched to real data.*

to a greater probability of high amplitude outliers. This tail is commonly observed in high resolution sea clutter measurements and is caused by the presence of sea spikes. Past studies have shown that the K distribution often provides a better fit to the real data [10, 11].

Figure 3 and 4 present the measured boat velocity and change of velocity, respectively, at each time step as measured using onboard GPS. It can be seen that the boat was manoeuvring strongly. It should also be noted that for approximately the first 10 scans the boat was moving very slowly after which time it rapidly accelerated to a velocity of greater than 10m/s (20 knots). A final observation is made on the SIR of the boat. During the early portion of the data set the signature of the boat is much less visible against the clutter background (not shown). After approximately 15 scans the relative strength of the target signal is seen to increase greatly with respect to the clutter background, probably due to a combination of changes in incidence and viewing angle.

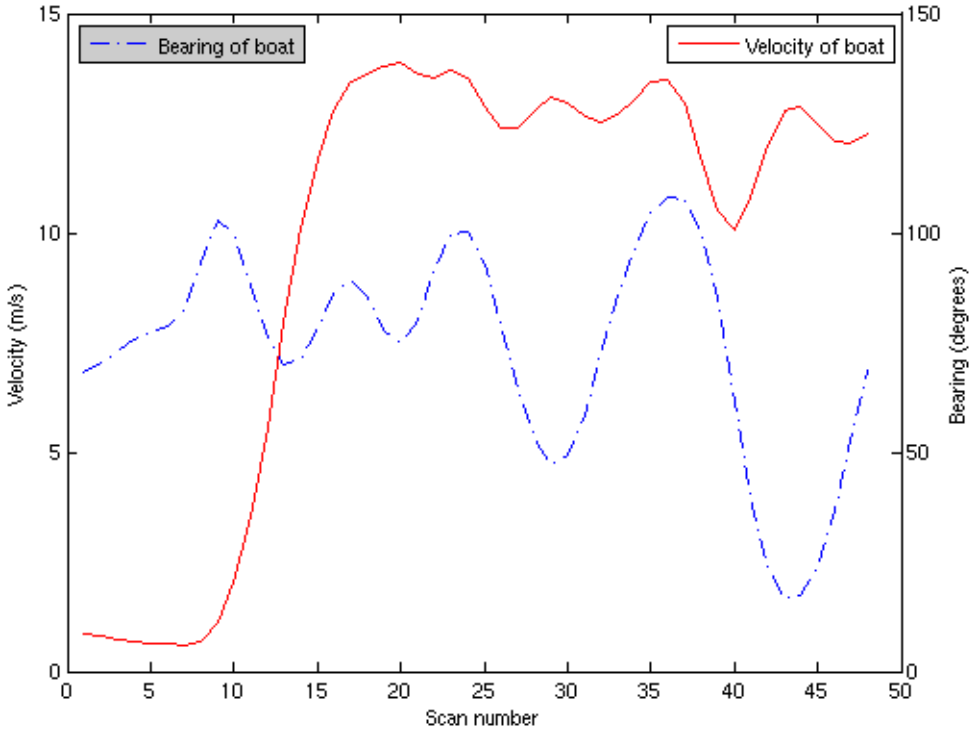

Figure 3: *Velocity and bearing of boat for each scan during trial collection period.*

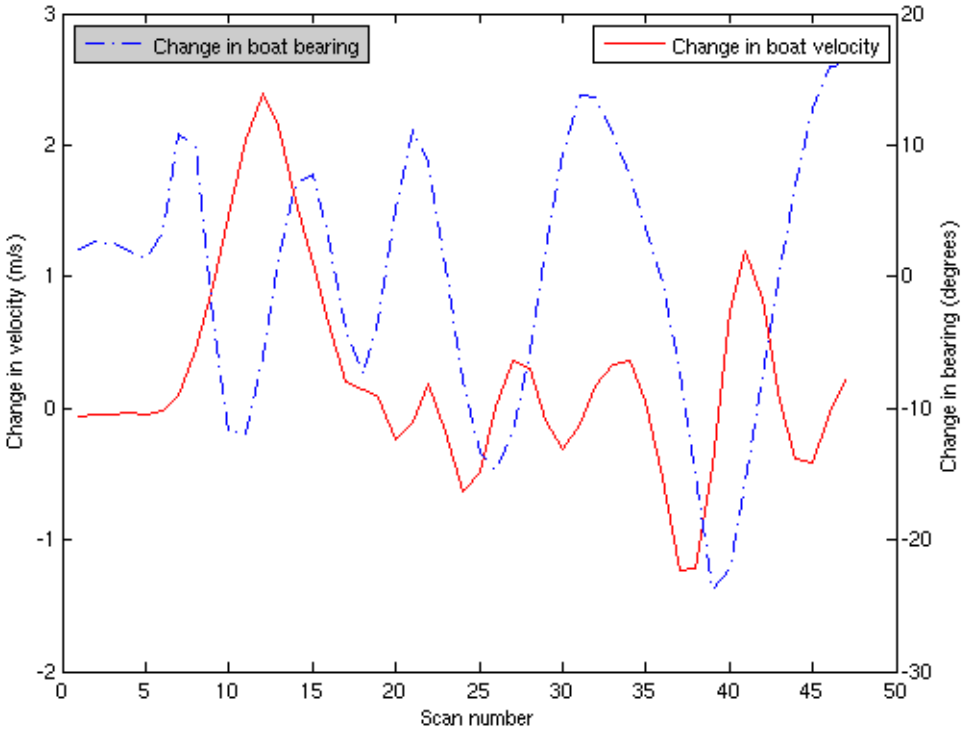

Figure 4: *Change of velocity and bearing of boat between scans of trial collection period.*

4 Examination of Diffusion and Constant Velocity Dynamic Models

In this section, we examine the implications of using a diffusion or constant velocity dynamic model as presented in equations 8 to 12.

4.1 Implementation of the Measurement Correction

The measurement correction corresponds to $p(y(tk)|x)$ in equation (4). Implementation of the measurement correction is difficult due to the departure of real life target and clutter characteristics from the analytically tractable stochastic models that must be used. Two PDFs commonly used to model radar clutter measurements are the Rayleigh and Gaussian PDFs. While it is apparent from the discussion of section 3.0 that the K distribution may provide a more accurate fit to the data, its application presents difficulties due to the lack of an analytical form for the target plus clutter distribution. In practice a numerical integration is required.

Further complications arise due to the choice of the target model. A common choice is the Swerling 0 target model, i.e. constant amplitude, as it significantly simplifies the measurement correction model. Unfortunately, highly manoeuvrable small cross-section targets tend to undergo very larger cross-section fluctuations from scan to scan and even from pulse to pulse. In recognition of this limitation, Rutten et al. [12] examined the application of the fading Swerling target models in Rayleigh clutter, while Hou and Morinaga [13] examined Swerling targets in K-distributed clutter.

Given the already high computational demands of implementing the Finite Difference (FD) approach and the desire to limit the computational requirements, the study in this section utilizes only the Gaussian and Rayleigh distributions with constant target amplitude.

It is easily shown that $p(y(tk)|x)$ corresponds to the calculation of the product of the likelihood ratios for each measurement point within the target spread function [14]. For the Gaussian distribution the likelihood ratio at each measurement point is given by

$$l\left(y^i(t_k)|x^n(t_k)\right) = \exp\left(\frac{2h_n^i y^i(t_k) - {h_n^i}^2}{2\sigma^2}\right), \tag{21}$$

where $y^i(t_k)$ is the measurement value at time t_k and position i, while h_n^i is the spread function value at position i for a target at position n. σ^2 is the variance of the Gaussian clutter.

The spread function, h_n^i , is assumed to be Gaussian in character for this report and is given

by

$$h_n^i = I \exp\left(-\frac{(x^i - x^n)^2 + (y^i - y^n)}{2\sigma_s^2}\right), \tag{22}$$

where x^i and y^i are the $x-$ and $y-$ location of the current measurement and x^n and y^n are the $x-$ and $y-$ location of the current state point. I is the actual amplitude of the target and σ_s^2 is the variance of the Gaussian spread function. In order to apply the Gaussian distribution it is necessary to remove the local mean from the measurements. This is done by subtracting the measured mean power of the measurement frame; the σ^2 is similarly calculated.

The likelihood ratio for the Rayleigh case is

$$l(y^i(t_k)|x^n(t_k)) = \exp\left(-\frac{(h_n^i)^2}{P}\right) I_0\left(\frac{2h_n^i y^i(t_k)}{P}\right), \tag{23}$$

where I_0 is a modified Bessel function of the first kind and P is the average Rayleigh clutter power determined by calculating the mean power across the measurement frame.

As part of the spread function calculation the target intensity, I, is required. This is typically not known a priori although a reasonable estimate may be formed through knowledge of desired target types. The implications of an incorrect choice of I can be profound and it is informative to examine the exponent of the Gaussian likelihood ratio to develop an understanding of the model sensitivity.

As I is made smaller the function h will shrink and the second term in the numerator of the exponent will approach zero. This causes the state density function to become cluttered with multiple local peaks corresponding to short lived clutter events such as sea spikes. In contrast, the effect of setting the I value too high will cause this same term to dominate resulting in suppression of the real target and enhancement of the larger clutter spikes. In the extreme case when I is set very high all likelihood ratios will be approximately equal, i.e., no measurement update occurs.

Even presuming the intensity value has been accurately chosen, significant performance degradation can still occur due to the mismatch between the real and postulated target plus clutter models. The most significant problems arise due to the enhanced high amplitude tail of the real clutter that was observed in Figure 2. Since neither the Gaussian nor the Rayleigh distributions 'anticipate' this increased prevalence of high amplitude clutter spikes they calculate a larger likelihood ratio then is warranted. The problem is further exacerbated by the fact that sea spikes share the same spread function as real targets as they arise due to localized reflections from long lived (seconds) wave fronts.

The result is that the filtered state probability distribution fails to maintain a 'lock' on the actual target location. Instead, the locations of the state distribution peaks fluctuate

rapidly from scan to scan, the latest peak location corresponding to the most recent clutter spike. The problem is compounded for very large spread functions, i.e., large number of measurement points. In this study, the observed 3dB width of the target spread function contains over 600 separate measurement points. Ideally, the more measurements the greater the integration gain but, in practise, the mismatch between the real and postulated target plus clutter models introduces a small error to each calculated likelihood ratio. These small errors translate into huge errors when the overall likelihood ratio is formed from the product of all individual likelihood ratios. The resulting overall likelihood ratios can be many order of magnitude larger then warranted. Care was taken during the processing in this report to restrict the extent of the spread function to prevent this exponential growth of the overall likelihood ratio error.

Error due to PDF mismatch must also be considered when designing an automatic detection algorithm. Attempts to implement a feedback mechanism that reduces the value of I when excessively large likelihood values are encountered will fail for the case where excessive likelihood ratios are actually due to PDF mismatch.

A simple ad hoc approach was adopted in this study whereby the value of the overall likelihood function was limited to a maximum upper value so as to suppress the effect of the largest clutter spikes. This approach was seen to provide a significant improvement in performance and is discussed in section 5.

4.2 Results

The data was processed across a 1.5 km by 1.25 km region with 100 grid steps in the x and y directions (i.e., 10^4 state points). For the CV model, an additional two dimensions, corresponding to the $x-$ and $y-$ velocities, are required. A relatively coarse velocity spacing corresponding to ± 40 m/s spread across 10 grid steps along the velocity dimensions is used. The CV state grid comprises 10^6 state points.

A 'detection' is determined as follows. The state density is summed across the velocity dimensions. The location of the maximum value of the collapsed state density is identified; the probabilities are then zeroed for all state points falling within ± 5 grid points. This zeroing acts as a crude multiple detection pruning technique. The process is repeated two more times until the maximum three state localities are identified.

The diffusion model is anticipated to be most suitable for slow moving targets. This observation is borne out by the results in Figures 5 and 6 for the two-dimensional Gaussian and Rayleigh diffusion models, respectively. Smaller dynamic variances allow the target to be detected during the early scans when the target is moving very slowly but has a weak SIR. Increasing the dynamic variance allows the target to be seen in the later scans where the target has accelerated but negatively impacts the detection performance during the early

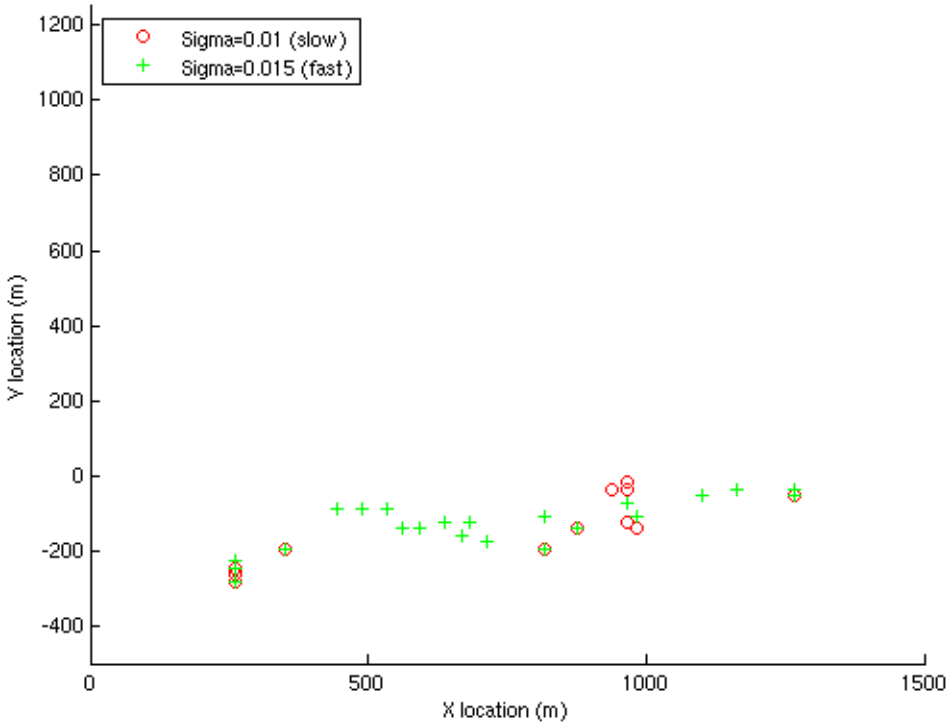

Figure 5: *Target detections after processing using diffusion model with assumption of Gaussian clutter.*

low SIR scans. This effect is particularly pronounced for Rayleigh processing where two distinct detection regimes are evident.

Figures 7 and 8 present the Gaussian and Rayleigh CV results. A general improvement in performance is observed with respect to the diffusion model with more consistent performance for all velocities and SIR conditions. While both techniques achieve some level of detection on virtually every scan, it is interesting to note the differences between the distributions of false target locations. False detections for the Gaussian approach are clustered more closely to the actual target path while for the Rayleigh case they are more randomly distributed. This has implications if the output of the FD processing is to be passed to a final Kalman tracker as the presence of more false detections close to the actual target path is likely to prove much more damaging to the final tracking solution.

Rayleigh CV processing results are also presented in Figure 8 for the case where no threshold limit is applied to the likelihood ratio. For this case the target is not detected at all during the first 18 scans corresponding to the time frame region in which the target SIR is low and there is a tendency for the state density to jump from clutter spike to clutter spike.

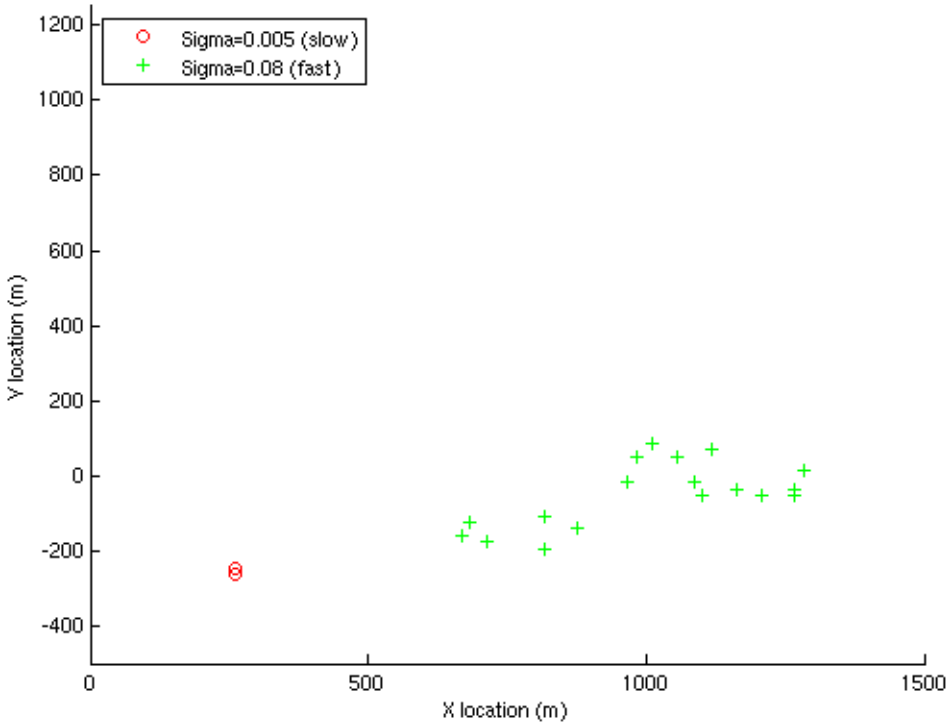

Figure 6: *Target detections after processing using diffusion model with assumption of Rayleigh clutter.*

Experimentation indicates that setting of threshold value is not especially sensitive and suitable values should be derivable using estimates of clutter power and desired target sizes.

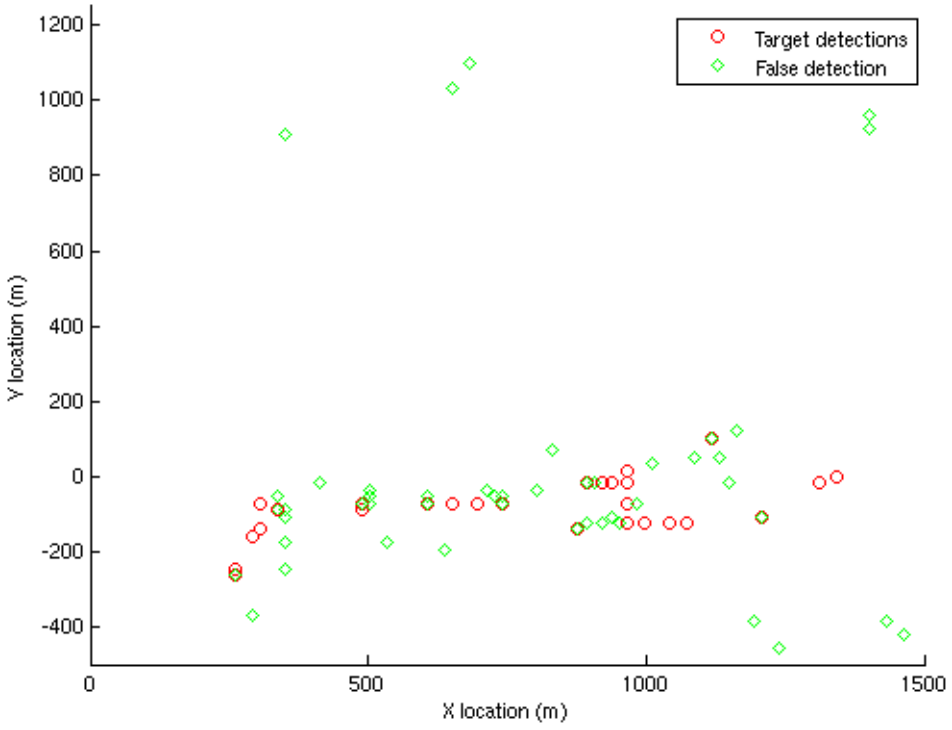

Figure 7: *Target detections and false detections after processing using constant velocity (CV) model with assumption of Gaussian clutter.*

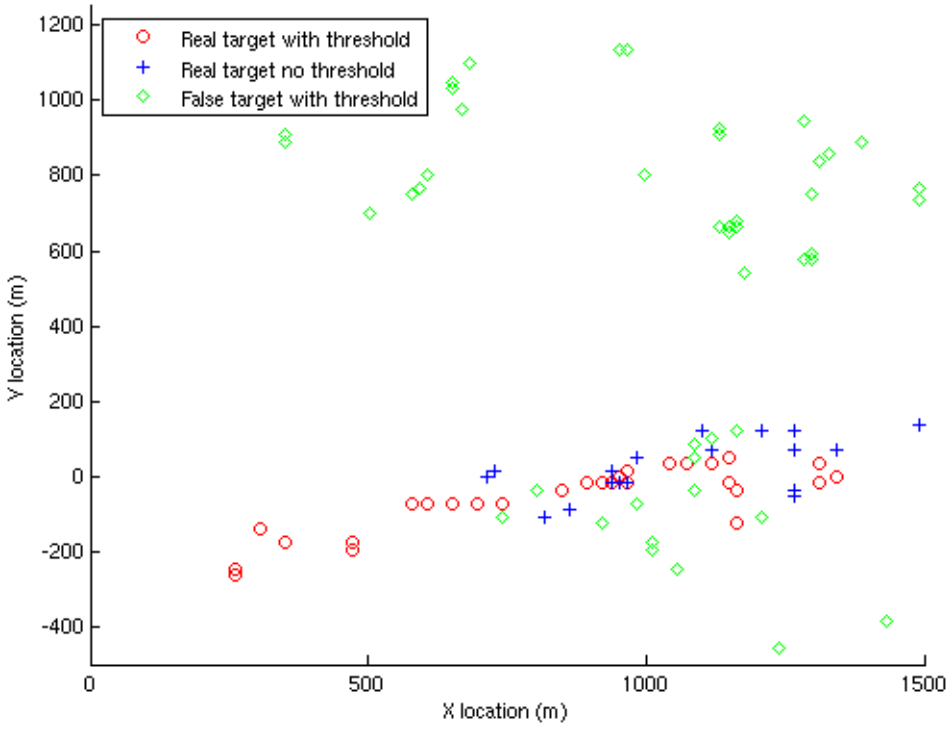

Figure 8: *Target detections and false detections after processing using constant velocity (CV) model with assumption of Rayleigh clutter.*

This page intentionally left blank.

5 Examination of Swerling Target Models

In this section, we examine the implications of assuming a Swerling 0, 1 or 3 target model during the formulation of the measurement model.

The measurement correction corresponds to the application of $p(y(t_k)|x)$ in Equation 4. In this section we will examine the application of a variety of commonly used target pdfs against the real data. To model the radar clutter we use the well-known Rayleigh pdf. As discussed earlier this choice tends to under-represent the proportion of high amplitude returns observed in the real data. While the K distribution appears to offer a slightly better fit, it does not permit a closed form expression for the signal plus noise pdf and requires the use of a numerical integration. This imposes a significant computational load and has not been implemented in this section. It will be examined in section 6. The implications of choosing the Rayleigh model are discussed further below.

A common choice for a target model is the Swerling 0, or constant amplitude, target model. Unfortunately, highly manoeuvrable small cross-section targets tend to undergo very large cross-section fluctuations between scan to scan and even between pulse to pulse measurements. In recognition of this limitation, Rutten et al. [12] suggested the application of the fading Swerling target models in Rayleigh clutter. In this section we implement models for a Swerling 1 and Swerling 3 target in Rayleigh clutter and compare it with Swerling 0 target results. While Rutten et al. indicated that the application of Swerling 1 and Swerling 3 models would necessitate the use of a numerical integral, this is not strictly true for the case where the measurement samples are statistically independent. For this case, simple closed form expressions are available for the Swerling 0 and Swerling 3 pdfs [15]. In general, the Swerling 1 target model is applicable to a complex target comprised of numerous independent scatterers of similar cross-section, while the Swerling 3 is representative of a target comprised of one large scatterer and numerous smaller cross section scatterers. The corresponding pdf for each target type is shown in Figure 9.

It is easily shown that calculating $p(y(t_k)|x)$ is equivalent to the calculation of the product of the likelihood ratios for each measurement point within the target spread function to within a common normalization factor [14]. The following sections detail the likelihood function corresponding to each of the clutter plus target models utilized in this study.

For all models the spread function of the target, h_n^i , is assumed to be Gaussian and is given by

$$h_n^i = I \exp\left[-\frac{(x^i - x^n)^2 + (y^i - y^n)^2}{2\sigma_s^2}\right], \tag{24}$$

where x^i and y^i are the x and y location of the current measurement and x^n and y^n are the x and y location of the current state point. I is the postulated amplitude of the target and

σ_s^2 is the variance of the Gaussian spread function. In regions where no component of the target spread function exists, the likelihood ratio reduces to a value of 1. It should again be emphasized that $p(y(t_k)|x)$ corresponds to the product of all the likelihood ratios formed from all the measurement locations (x^i and y^i) within the spread function, i.e.,

$$l(y(t_k)|x^n(t_k)) = \prod_i \frac{p(y^i(t_k)|x^n(t_k), H_1)}{p(y^i(t_k)|x^n(t_k), H_0)}, \tag{25}$$

where H_1 and H_0 denote the cases where the target is present and where the target is not present, respectively.

5.1 Rayleigh distribution Model with Swerling 0 Target

The pdf for a Swerling 0 target in Rayleigh clutter is given by

$$p(y^i(t_k)|x^n(t_k), H_1) = \frac{2y^i(t_k)}{P} \exp\left(-\frac{y^i(t_k)^2 + (h_n^i)^2}{P}\right) I_0\left(\frac{2h_n^i y^i(t_k)}{P}\right), \tag{26}$$

(see, for instance, [12]) where I_0 is a modified Bessel function of the first kind and P is the average Rayleigh clutter power determined by calculating the mean power across the measurement frame. The pdf for Rayleigh clutter without a target is given by

$$p(y^i(t_k)|x^n(t_k), H_0) = \frac{2y^i(t_k)}{P} \exp\left(-\frac{y^i(t_k)^2}{P}\right). \tag{27}$$

The corresponding likelihood ratio for the Rayleigh case is therefore given by

$$l(y^i(t_k)|x^n(t_k)) = \exp\left(-\frac{(h_n^i)^2}{P}\right) I_0\left(\frac{2h_n^i y^i(t_k)}{P}\right). \tag{28}$$

5.2 Rayleigh Distribution Model with Swerling 1 Target

The pdf for a Swerling 1 target in Rayleigh clutter is given by

$$p(y^i(t_k)|x^n(t_k), H_1) = \left(1 + \frac{(h_n^i)^2}{P}\right) \exp\left(-\frac{y^i(t_k)^2}{P + (h_n^i)^2}\right), \tag{29}$$

where the intensity used in calculation now corresponds to the average target intensity[15]. The corresponding likelihood ratio is formed using Equations 27 and 29.

5.3 Rayleigh Distribution Model with Swerling 3 Target

The pdf for a Swerling 3 target in Rayleigh clutter is given by

$$p(y^i(t_k)|x^n(t_k), H_1) = \frac{1}{\left(1+\frac{(h_n^i)^2}{2P}\right)}\left[1+\frac{\frac{y^i(t_k)^2}{P}}{\left(1+\frac{2P}{(h_n^i)^2}\right)}\right]\exp\left[-\frac{\frac{y^i(t_k)^2}{P}}{\left(1+\frac{(h_n^i)^2}{2P}\right)}\right], \qquad (30)$$

where the intensity used in calculation now corresponds to the average target intensity[15]. The corresponding likelihood ratio is formed using Equations 27 and 30.

5.4 Comments

To calculate the spread function the target intensity, I, is required. This is typically not known a priori although a reasonable estimate may be formed through knowledge of desired target types. Methodologies for choosing an optimum intensity value are not examined in this paper, rather, an optimum intensity value is determined by trial and error. For the purposes of this study, the optimum intensity is considered to be that which achieves target detection on the maximum number of scans. The concept of a 'detection' is discussed in further detail in Section 5.5 below. In all cases the target intensity is held constant across all scans.

Even presuming the optimum intensity value has been accurately chosen, significant performance degradation can still occur due to the mismatch between the real and postulated target plus clutter models. Significant problems arise due to the enhanced high amplitude tail of the real clutter that was observed in Figure 2. Since the Rayleigh distribution does not 'anticipate' this increased prevalence of high amplitude clutter spikes it produces a larger likelihood ratio than is warranted.

The result is a filtered state probability distribution, which fails to maintain a 'lock' on the actual target location. Instead, the locations of the state distribution peaks fluctuate rapidly from scan to scan, the latest peak location corresponding to the most recent clutter spike. The problem is compounded for very large spread functions, i.e., large number of measurement points. In this study, the observed 3 dB width of the target spread function contains over 600 separate measurement points. Ideally, more measurements will result in greater integration gain; however, in practise the mismatch between the real and postulated target plus clutter models introduces a small error to each calculated likelihood ratio. These small errors translate into huge errors when the overall likelihood ratio is formed from the product of all individual likelihood ratios. The resulting overall likelihood ratios can be many order of magnitude larger then warranted. Care was taken during the processing in this analysis to restrict the extent of the spread function in order to prevent this exponential growth of overall likelihood ratio error. In addition, a simple ad hoc approach was adopted in this study whereby the value of the overall likelihood function was limited to a maximum

upper value so as to suppress the effect of the largest clutter spikes. This approach was seen to provide a significant improvement in performance. All three target models were observed to exhibit similar performance gains when likelihood limiting was employed.

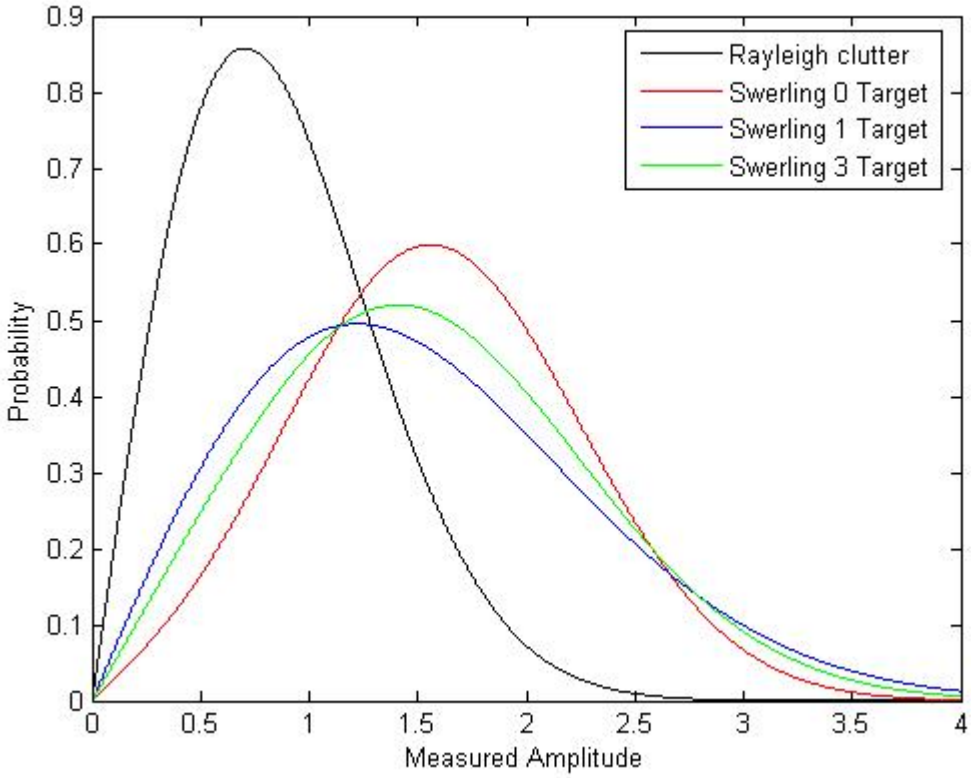

Figure 9: *Sample probability distribution function curves for pure Rayleigh clutter and Swerling 0, 1 and 3 targets in Rayleigh clutter. Average target signal power is 3 dB above clutter power.*

It is instructive to further examine the properties of the Swerling target models with respect to one another. Figure 9 presents the pdf curves for Swerling 0, 1 and 3 targets in Rayleigh clutter. As anticipated, the Swerling 1 and 3 distributions exhibit a larger variance than the Swerling 0 target model, with the Swerling 1 being the broadest. The effect of increased variance on the calculated likelihood ratio is illustrated in Figures 10 and 11.

From Figure 10 it is observed that likelihood ratios of the Swerling 0 model are most sensitive to the average target power assumption (corresponds to choosing intensity, I, in the spread function calculation detailed above) while the Swerling 1 model is least sensitive. In a practical implementation, the choice of a correct target power is not a trivial task and the apparent desensitization of this parameter could prove highly advantageous. The converse of the relationship is illustrated in Figure 11, where the likelihood ratio is plotted against

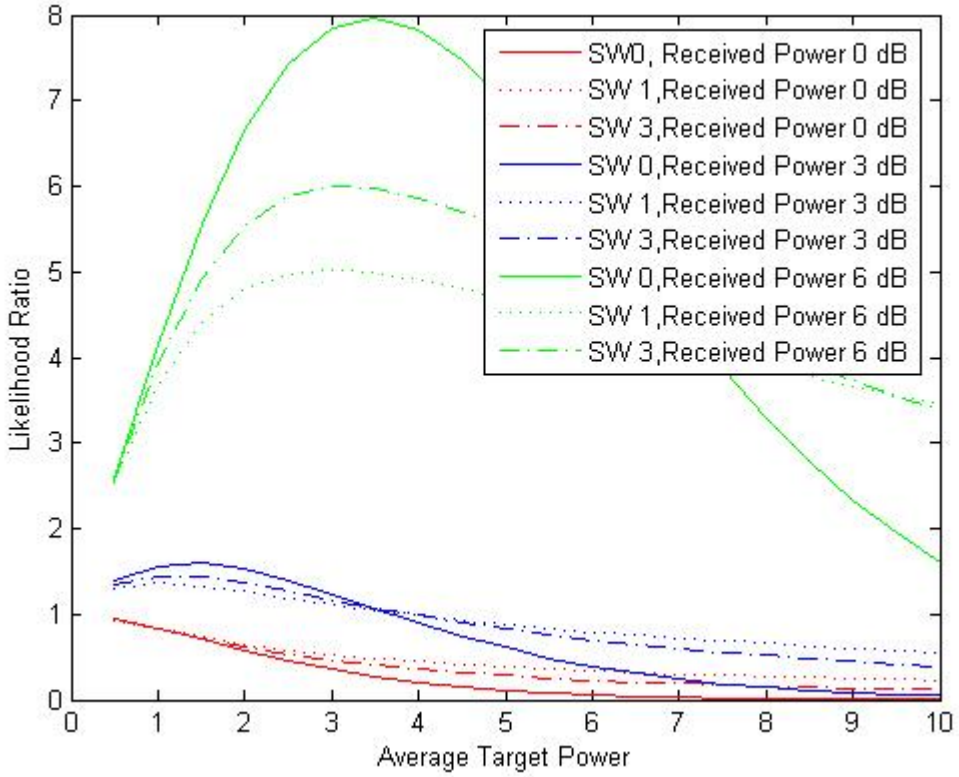

Figure 10: *Variation of calculated likelihood ratio against postulated average target power for received measurement powers of 0 dB, 3dB and 6dB above clutter power. Curves are shown for Swerling 0, 1 and 3 target models.*

received power for a fixed underlying target power. It is readily observed that the Swerling 0 target model provides the most aggressive promotion and demotion of the posterior density. Namely, when a weak signal power is observed the posterior density is more heavily suppressed (i.e., the likelihood ratio is less then one) while for strong signals the posterior is most strongly promoted (i.e. likelihood ratio greater then one). While the difference in individual likelihood ratios between Swerling models may appear small, it can become very large when the product of a large number of likelihood ratios is computed to determine the overall likelihood ratio.

Neither of the above behaviours is unexpected but must be fully appreciated when comparing results via different target models. In practical terms one would expect to find that the posterior distributions associated with Swerling 0 targets would be more strongly peaked then those with the Swerling 1 and 3 targets. The broader the variance of the underlying target model, the flatter the expected posterior distribution. The temporal behaviour of the posterior evolution is also likely to differ; the low variance Swerling 0 model will likely show

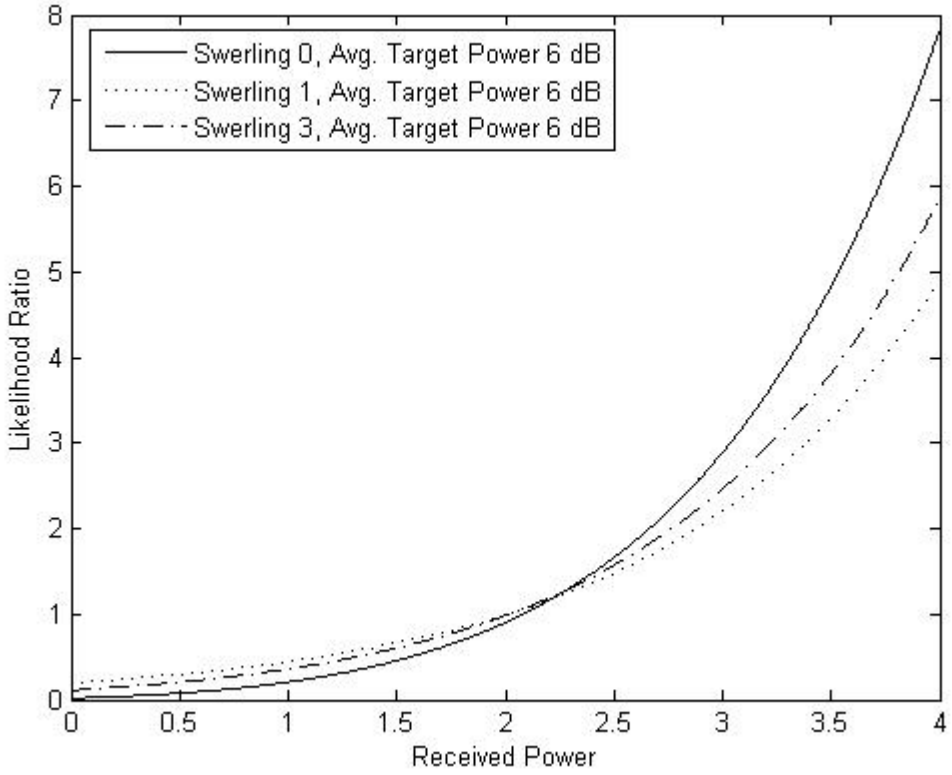

Figure 11: *Variation of calculated likelihood ratios against received measurement power for postulated average target power 6dB above clutter power.*

a greater sensitivity to anomalous clutter peaks (with an associated peak in the posterior) but the signature of transient events will more rapidly decay with time due to the greater subsequent suppression.

5.5 Results

The data was processed across a 1.5 km by 1.25 km region with 100 grid steps in the $x-$ and $y-$ directions (i.e., 10^4 state points). For a CV model, an additional two dimensions, corresponding to the $x-$ and $y-$ velocities, are also required. A relatively coarse velocity spacing corresponding to ± 40 m/s spread across 10 grid steps along the velocity dimensions was used. The CV state grid thus comprises 10^6 state points.

A 'detection' was determined as follows. The state density was summed across the velocity dimensions. The location of the maximum value of the collapsed state density was identified and the probabilities were then zeroed for all state points falling within ± 5 grid points. This

zeroing acts as a crude multiple detection pruning technique. The process can be repeated to extract progressively smaller maximum state localities. In the following text, detections will be referred to as a first maximum detection, second maximum detection etc. to identify the order of extraction.

It should be noted that while this approach bears some passing resemblance to the concept of specifying a given Probability of False Alarm (PFA) in that choosing one mode crudely corresponds to a PFA of 1/# of independent state locations. Allowing three modes would correspond to 3/# of independent state locations, etc. However, this approach is not strictly Constant False Alarm Rate (CFAR). In addition, this concept of modal 'detection' differs from the more commonly utilized approach of applying a threshold to the measured target amplitude in a number of subtle but significant ways.

The first important difference is that the output of the TkBD processing is a posterior measure of the probability that the target is present at a given location within the field of view rather than some function of the current measured radar return. The posterior measure reflects the entire history of measurements up to that point in time, hence, it is more representative of a track then an individual detection and the applicability of detection performance measures such as the probability of detection (PD) and the PFA become much less clearly defined. Characterization of tracking performance is a much more difficult problem than detection performance and one is typically forced to resort to a broad range of measures such as false track rate, false track length, association changes, missed object history, omitted tracks, track establishment delay and so on to quantitatively capture the results. In most cases there is not one definitive combination of specifications that characterize ideal performance, rather, the tracker designer must choose the mixture that best suits their application. This sort of analysis is beyond the scope of this study and is, in fact, not possible here due to the limited size of the data set and the inability to calculate statistically meaningful values.

As will be discussed later, it is envisioned by the authors that a practical implementation of TkBD would require a follow-on tracker stage to refine the tracklet input from the TkBD and identify the real target tracks. Under this scenario the overall performance is an intimately coupled function of the TkBD and follow-on tracker design. Further investigations of these aspects are reserved as a topic for future study. The focus of the following discussion is to highlight the impact of utilizing different target models and, in particular, understand the effect of this choice on the posterior and the distribution of modes within it. General observations of how posterior distributions and modal 'detections' are affected by target choice are presented but definitive statements on the superiority of one model with respect to another cannot be provided for the reasons discussed above.

Figure 12 compares results obtained using a Swerling 0, 1 and 3 target model. To generate this plot, the top three maximum detection localities have been identified on each scan. Only the detections that clearly coincide with the actual target location (as determined by GPS

truth and raw signal intensity plots) are retained and plotted.

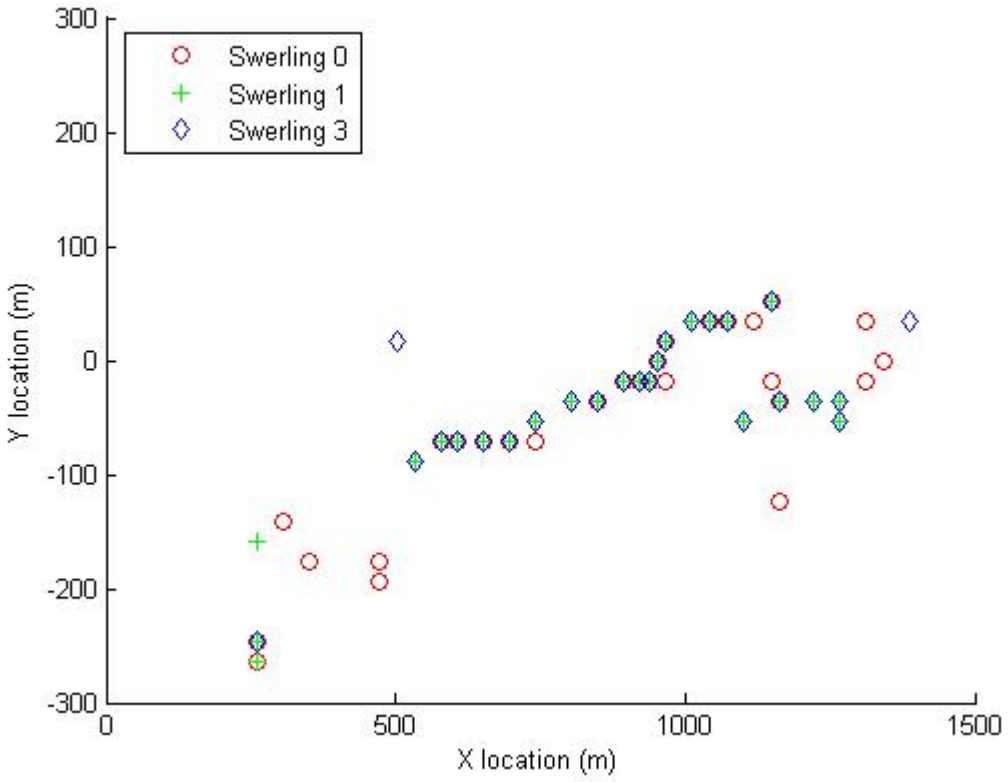

Figure 12: *True target detections for Swerling 0, 1 and 3 target models when top three maximum localities are considered.*

It is evident from Figure 12 that the Swerling 0 target provides the greatest detection performance as it successfully detects the target on almost all scans. The Swerling 1 and 3 models, which produce virtually identical results to each, suffer from large drop out regions, particularly near the beginning of the data set, in which the target is not detected. At first glance this result seems somewhat surprising as the Swerling 0 target model permits the smallest variation in target signal and would be expected to be least tolerant of changes in target strength across the data set. Figure 13 sheds further light on this discrepancy. In Figure 13, only the first maximum detection from each scan is extracted and only those detections corresponding to the actual target are plotted in the figure. The result is a strong degradation of Swerling 0 target model performance with respect to the Swerling 1 and 3 models in comparison with that observed in Figure 12. It is difficult to be definitive on the precise mechanisms at work due to the complicated environmental conditions, but some of the differences are likely explained by the enhanced promotion/demotion characteristics of the Swerling 0 target model discussed above. The ability of the Swerling 0 target model to provide second or third maximum detections of the target reflects its greater sensitivity

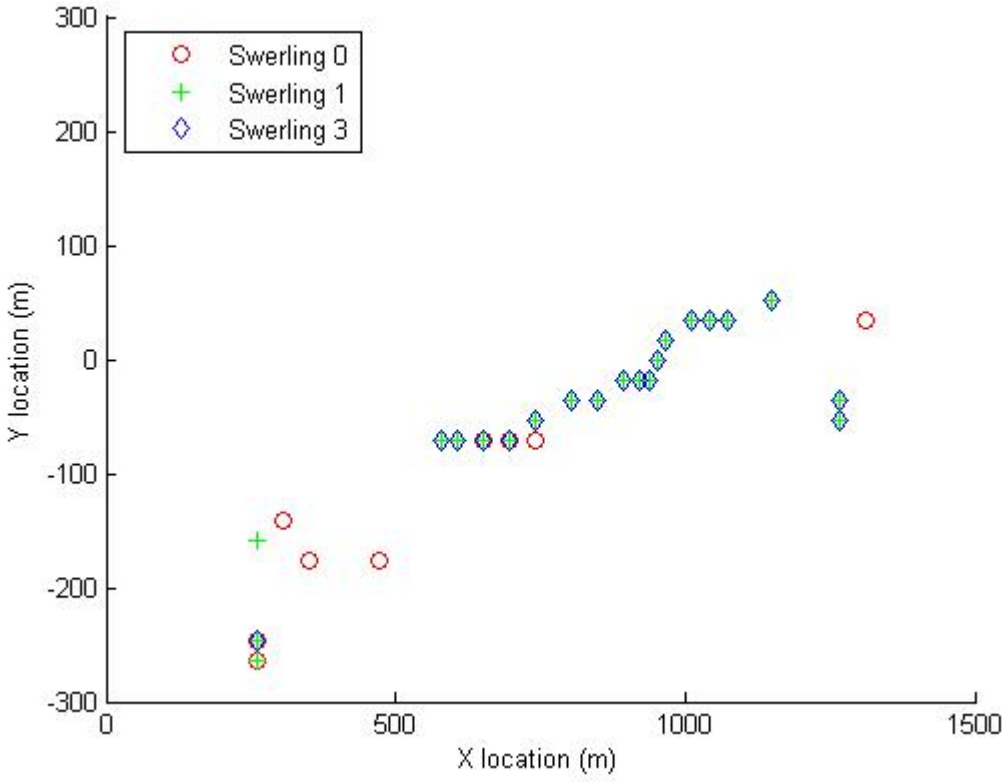

Figure 13: *True target detections for Swerling 0, 1 and 3 target model when only first maximum is considered.*

to small changes in received signal strength. This effect should be evident as a strongly peaked posterior distribution. The difference between the target models is likely to be most pronounced during the earlier scans when the target signal was observed to be much weaker and less stable and in fact, it is in this time frame that the Swerling 1 and 3 targets suffer from a detection drop out. However, the enhanced sensitivity also means that the approach is more sensitive to clutter spikes, hence the increased prevalence of second or third maximum detections of the actual target in later scans.

Figures 14 and 15 present sample contour plots of the posterior density for one scan derived using the Swerling 0 and Swerling 1 target models respectively. The Swerling 3 results are very similar to the Swerling 1 results and are omitted for conciseness. The enhanced multi-modal character of the Swerling 0 results with respect to the Swerling 1 results is readily apparent and supports the discussion above.

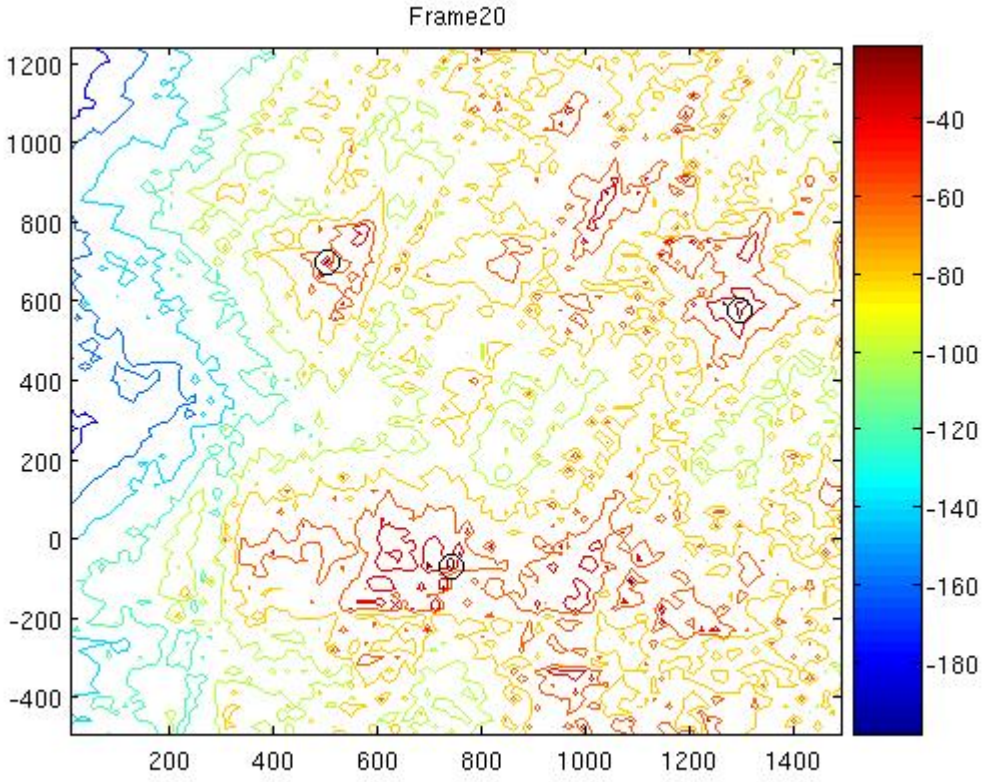

Figure 14: *Contour plot of posterior density function for Swerling 0 model on selected scan.*

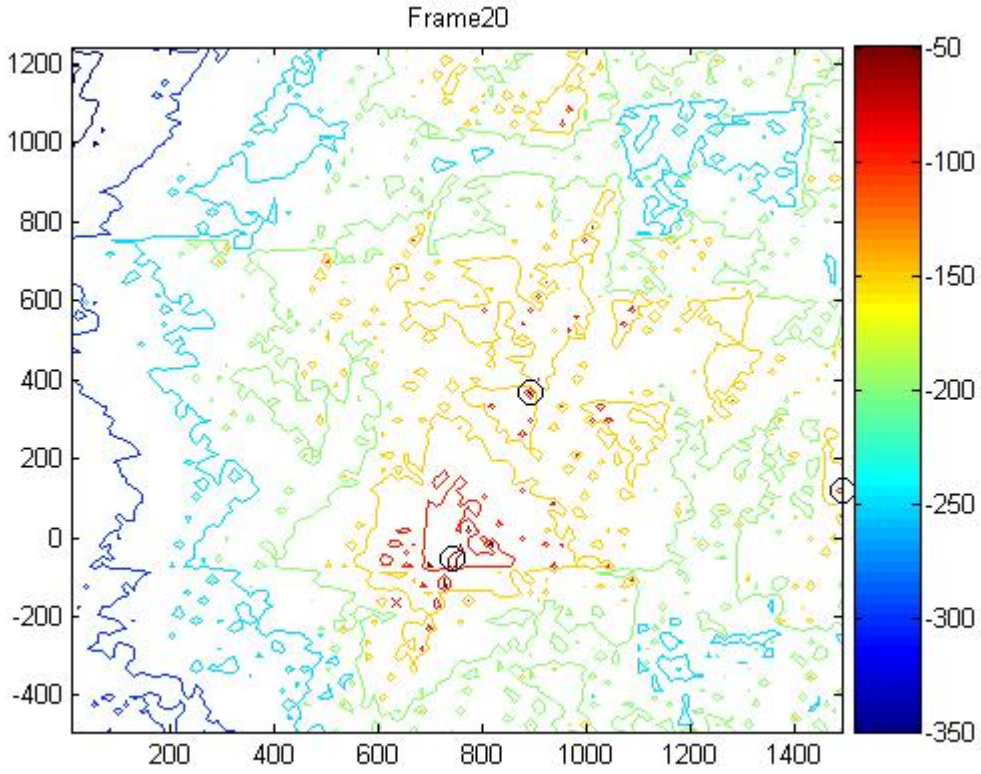

Figure 15: *Contour plot of posterior density function for Swerling 1 model on selected scan.*

This page intentionally left blank.

6 Examination of Clutter Models

In this section, we examine the implications of using different stochastic models to describe the underlying clutter signal. Simulated data was generated to provide a baseline of comparison for the results obtained from the real data. Three simulated data sets were generated corresponding to clutter possessing Rayleigh, K-distributed and KA-distributed pdfs [16, 17]. All aspects of spatial distribution, time steps, etc., were set to be identical to the real data. A Swerling 0 target was embedded in clutter following an identical trajectory to the target in the real data set as determined from GPS truth data recorded on board the boat during the trial. The spread function associated with the antenna beam pattern was imposed on the target signal and, in the case of the KA distribution, on the discrete clutter spikes. The goal was to reproduce the target dynamics as closely as possible while controlling the clutter and target pdfs.

6.1 Measurement Correction

The measurement correction corresponds to the application of $p(y(t_k)|x)$ in Equation 4. In this section three different pdfs will be used to model clutter behaviours: Rayleigh, K and KA distributions. In all cases a Swerling 1 (i.e., constant amplitude) model is assumed. As discussed in section 5 this model was previously seen to produce the most robust results for the real data examined in this study. The calculation of the likelihood ratio for each of the above models is described in detail below and any implementation issues discussed.

Figure 16 presents a sample of typical PFA versus Threshold curves achieved by fitting the above pdfs to real data. It is readily apparent that the Rayleigh clutter model fails to adequately capture the frequency of high amplitude clutter events. It is well known that high resolution radar measurements of sea clutter frequently display this spiky behaviour [16, 17]. These sea spikes are particularly troublesome due to their relatively long persistence (on the order of seconds) and the corresponding difficulty of removing them through integration. The K and KA distributions have been proposed as pdfs which provide improved fits to real data. Referring to Figure 16, we can also see the curves that are produced when the K and KA distributions are fitted to the real data. Clearly, the K, and especially the KA pdf, provide a much better match. The drawback is that both approaches are computationally more demanding and, in addition, the KA distribution requires the specification of multiple parameters which are not easily derived from the data. As a crude measure of computational effort it is noted that our Matlab code for the Rayleigh likelihood calculation would take on the order of hours to run while our KA likelihood calculation would take on the order of days, a roughly two orders of magnitude difference.

The calculation of the likelihood ratio for each of the above pdfs is described in detail below along with implementation issues. The spread function of the target, h_n^i, is again assumed to be Gaussian and is given by 24.

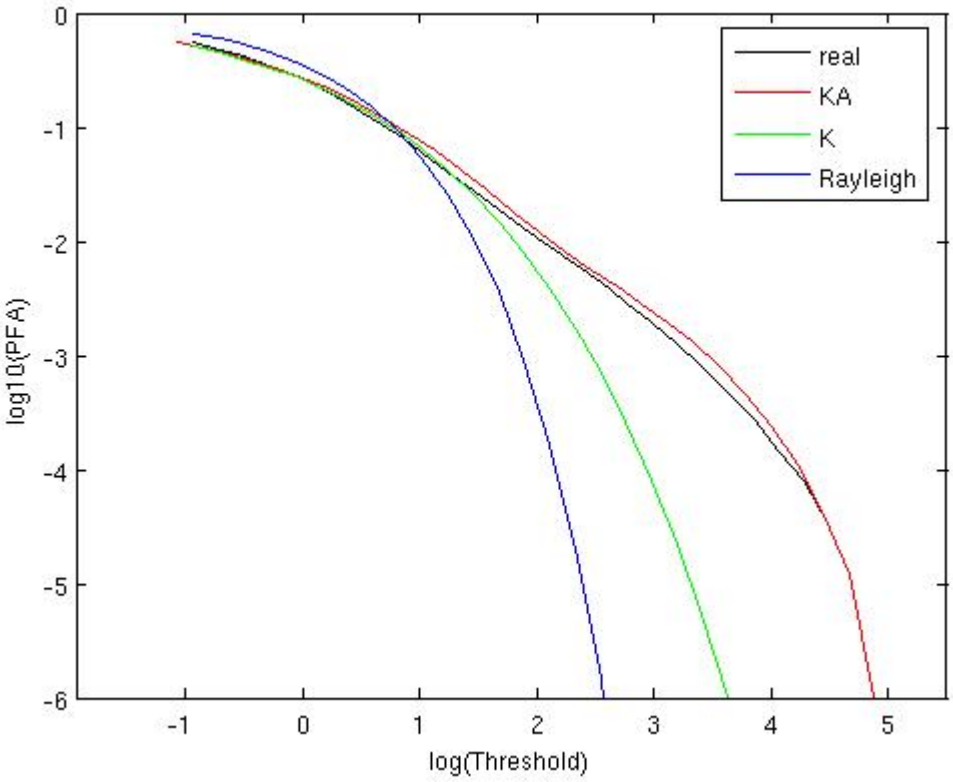

Figure 16: *Probability of false alarm (PFA) versus threshold for real data sets and as predicted by Rayleigh, K and KA distributions fitted to real data.*

6.2 Rayleigh distribution model with Swerling 0 Target

The likelihood ratio for the Rayleigh case is easily derived and given by

$$l(y|\langle P\rangle, h_n^i) = \exp\left(-\frac{(h_n^i)^2}{\langle P\rangle}\right) I_0\left(\frac{2h_n^i y}{\langle P\rangle}\right), \tag{31}$$

where $\langle P\rangle$ is the average clutter power and y is the measured amplitude of the signal [12].

6.3 $K-$distribution model with Swerling 0 Target

The K-distribution belongs to a broader class of distribution known as the compound Gaussian given by

$$p(y|\langle P\rangle, h_n^i) = \int_0^\infty \frac{2y}{P} \exp\left(-\frac{y^2}{P}\right) p(P|\langle P\rangle) dP, \tag{32}$$

where the value P corresponds to the local underlying power of the clutter and $\langle P \rangle$ is the average clutter power of the distribution $p(P|\langle P \rangle)$. The corresponding target plus clutter distribution is given by

$$p(y|P, h_n^i) = \int_0^\infty \frac{2y}{P} \exp\left(-\frac{(y^2 + h_n^i)^2}{P}\right) I_0\left(\frac{2yh_n^i}{P}\right) p(P|\langle P \rangle) dP. \tag{33}$$

If the distribution of the P variable is specified as the gamma distribution the K-distribution results, i.e.,

$$p(P|\langle P \rangle) = \frac{1}{\Gamma(\nu)} \left(\frac{\nu}{\langle P \rangle}\right)^\nu P^{\nu-1} \exp\left(-\frac{\nu P}{\langle P \rangle}\right) dP, \tag{34}$$

where ν is the shape parameter. For the case where no target is present Equation 32 admits a closed form solution of the form

$$p(y) = \frac{\pi\nu}{\Gamma(\nu)\langle P \rangle} \left(\sqrt{\frac{\pi\nu}{4\langle P \rangle}}\right)^{\nu-1} K_{\nu-1}\left(\sqrt{\frac{\pi\nu}{\langle P \rangle}}\right). \tag{35}$$

Unfortunately no closed form solution exists for the Swerling 0 target case and the integral in Equation 33 must be evalutated numerically. For this study a Monte Carlo sampling approach was implemented and the evaluation was performed using 100 samples of P drawn from the gamma distribution. The shape parameter of the real data was estimated using the $z \log z$ method [18]; this approach tends to ignore the contribution of Guassian white noise to the signal but is considered sufficiently accurate for this data set in which the returns are strongly clutter limited.

6.4 KA-distribution model with Swerling 0 Target

The KA distribution was initially suggested by Ward and Tough [16] as a good candidate to more accurately model sea clutter distributions. The pdf of the KA distribution is given by

$$p(y|P, n, \sigma_{sp}) = \sum_{n=0}^{\infty} \frac{y}{P + n\sigma_{sp}} \exp\left(-\frac{y^2}{P + n\sigma_{sp}}\right) P_{pois}(n|\bar{N}), \tag{36}$$

where n is the number of spikes in a given range cell, σ_{sp} is the mean spike intensity and $\bar{N}$ is the average number of spikes in a given range cell. In essence, the KA-distribution represents a K distribution to which random spike events have been added. As such, $p(y|H_0)$ and $p(y|H_1)$ can be determined in similar fashion to the K distribution using Equation 33. In practice $\bar{N} \ll 1$ so that only the first two terms of the summation need to be evaluated. It is seen that the $n = 1$ term of the summation is easily evaluated by substituting $P + n\sigma_{sp}$

for the P term in the denominators of the terms in Equation 33, i.e.,

$$p(y|P,h_n^i,n,\omega_{sp}) = \sum_{n=0}^{\infty}\Bigg[\int_0^{\infty} dP \frac{2y}{P+n\sigma_{sp}} \times \exp\left(-\frac{(y^2+(h_n^i)^2)}{P+n\sigma_{sp}}\right) I_0\left(\frac{2ys}{P+n\sigma_{sp}}\right) p(P)\Bigg] P_{poiss}(n|\bar{N}). \tag{37}$$

The calculation of the KA terms requires the determination of σ_{sp} and N. For this study the parameters were determined through the trial and error fitting process described by Watts et al. [17]. The determination of these parameters is difficult and represents a significant barrier to practical implementation of the approach.

6.5 Results from Simulated Data

Each of the simulated data sets was processed using a TkBD algorithm with the measurement correction step perfectly matched to the clutter characteristics of the simulated data. In all cases excellent performance was noted with successful detection and tracking of the target typically achieved after only a few measurements. This cross-check provides a high degree of confidence that the dynamic model chosen to represent the target dynamics is representative of the target and will lead to a stable TkBD solution provided the measurement correction is properly implemented. This is an important point as a poor choice of dynamic model could lead to poor TkBD performance even when the clutter pdfs are perfectly known.

The sensitivity to choice of clutter pdf was investigated by processing the simulated KA-distributed data set using TkBD processors employing Rayleigh, K and KA based measurement corrections. Not surprisingly, the Rayleigh based TkBD displayed the worst performance, appearing to correctly locate the target on only a few isolated scans. The K based TkBD performed much better. It required approximately 10 scans to lock onto the target but after achieving this initial lock it maintained this 'track' until the end of the data set at scan 39. The KA based TkBD gave the best performance and locked onto the target within two scans and maintained a 'track' across the entire data set.

These results illustrate the significant sensitivity of TkBD performance to clutter models and the improvements in TkBD performance that can be achieved if the clutter models and real life clutter characteristics are closely matched. However, as will be seen in the next section, this potential for improved detection performance appears to come at a cost of greater sensitivity to mismatches between the idealized models and real behaviour, i.e., while perfectly matched models provide excellent results, small mismatches can lead to catastrophic performance degradation. In effect, the processor becomes highly tuned to a particular model.

6.6 Results from Real Data

Referring to Figure 16 we again note the excellent fit between the real data PFA versus threshold curve and that generated using the KA distribution. Given the implied similarity of the simulated KA data and the real data, coupled with the demonstrated excellent performance of the KA and K based tracker on the simulated data, there is a natural tendency to conclude the TkBD performance against the real data set is likely to be greatly improved by inclusion of the K and, even more so, the KA pdf model into the corrections step. Unfortunately this did not prove to be the case.

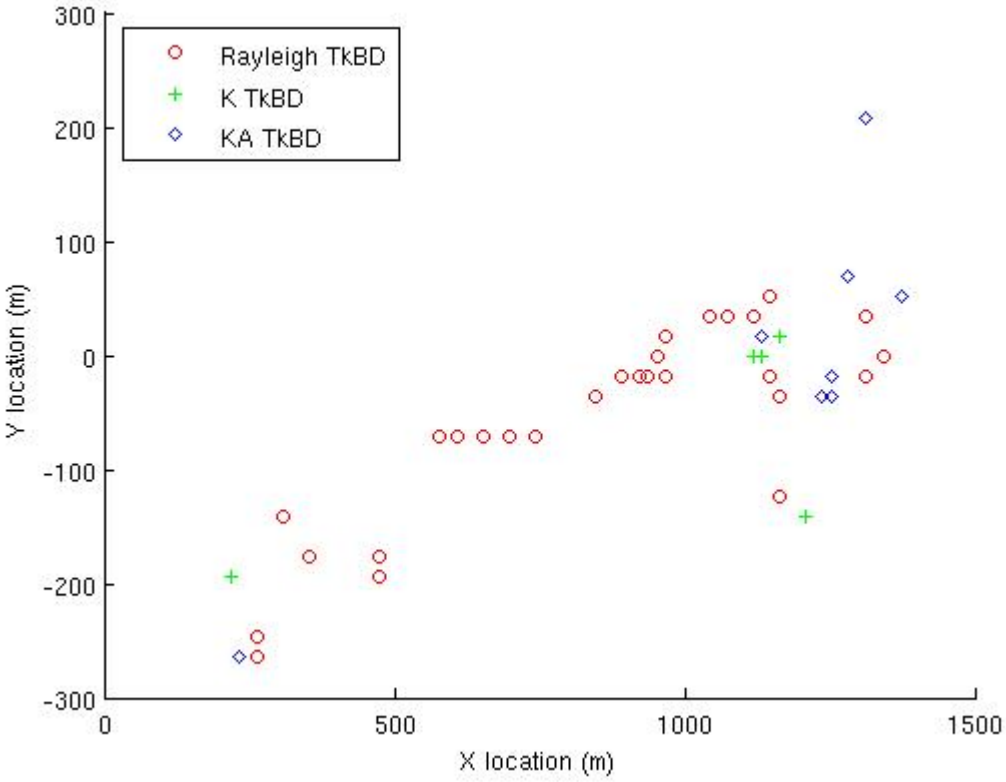

Figure 17: *Target detections after processing using Rayleigh, K and KA based Track Before Detect (TkBD) processor.*

Figure 17 presents the detection results from applying the Rayleigh, K and KA based TkBD to the real data sets. As with previous sections it was found to be useful to define a 'detection' as follows. The state density is summed across the velocity dimensions. The location of the maximum value of the collapsed state density is identified and the probabilities are then zeroed for all state points falling within ± 5 grid points. This zeroing acts as a crude multiple detection pruning technique. The process is repeated two more times until the maximum

three state 'localities' or detections are identified. Only the mode locations corresponding to the actual target location are plotted in Figure 17.

It was previously shown that the introduction of a simple limiting step to the likelihood ratio calculation produced a significant improvement in Rayleigh based TkBD performance as it diminished the impact of high amplitude spike events on the final solution [19, 20]. This approach is implemented for the Rayleigh based processing. A discussion of why this limiting step is reasonable and required is provided below.

It is readily observed in Figure 17 that the Rayleigh TkBD provides excellent results with target 'detection' occurring on almost every scan. The same cannot be said of either the K or KA based TkBD. Both methods perform poorly, failing to detect the target location until the final five to eight scans.

The complexity of the real clutter (and target) environment makes it difficult to provide definitive reasons for the failure of these apparently more sophisticated and accurate clutter models, but an examination of the behaviour of the likelihood ratio calculations provides insight into at least some of the reasons.

Figure 18 presents a plot displaying a series of likelihood ratio values versus actual measured value curves for a single point within a scan as determined using K-distributed and Rayleigh distributed clutter models. One of the most readily evident features is the monotonically increasing nature of the Rayleigh curve. This behaviour readily explains the usefulness of the likelihood limiting step discussed above. The presence of high amplitude clutter spike events results in the calculation of unrealistically large likelihood ratios. When the corresponding overall likelihood ratios are computed from the product of hundreds of similar individual likelihood ratios it leads to astronomically large values. The end result is that the posterior is overwhelmingly dominated by the latest clutter events. Limiting the overall likelihood ratios forces target and spike events to have similar impacts on the correction step. Examination of the K distribution curves in Figure 18 reveals that the introduction of a similar limiting step for K and KA based processing is likely to be unsuccessful as the curves are no longer monotonic and the peak of the likelihood ratio occurs in the measurement range where the real targets are likely to dominate. Large amplitude clutter spikes are already inherently suppressed by the pdf model. Attempts to limit likelihood values are therefore more likely to suppress measurements associated with a real target then those associated with large clutter spikes.

The net result is that there is no simple ad hoc approach to compensate for discrepancies between the real clutter characteristics and the K or KA models that are used. As such, the models need to be carefully matched as small discrepancies can lead to large errors in the calculation of the overall likelihood ratio. This can be illustrated by an examination of the curves corresponding to v=0.1 and v=0.5 in Figure 18. Examination of the peak of the curves in the regions near the measured value of 1.2 reveal a difference of approximately 20% in the calculated likelihood ratio. In other words, an incorrect choice of shape parameter

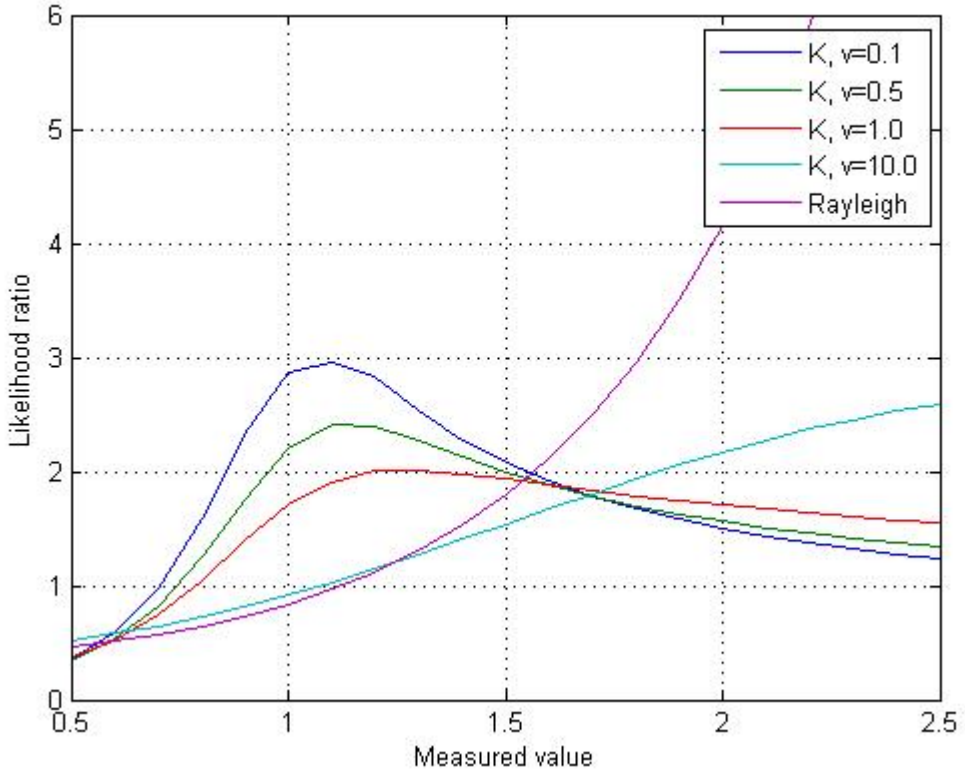

Figure 18: *Variation of likelihood ratio versus measured signal value for clutter statistics assumed to follow Rayleigh probability density function and K distribution for shape parameters of 0.1, 0.5, 1.0 and 10. Postulated target intensity is held constant at 1.0 and mean clutter power is held constant at 1.0.*

can lead to an error of 20% in the calculated likelihood ratio. Clearly, this could lead to a massive under-assessment of the significance of a target measurement when the product of hundreds of similarly affected likelihood ratios is calculated.

In general terms, this illustrates the double-edged sword nature of implementing non-linear TkBD methods. While the distributed nature of the target spread function (and associated non-linearity of the measurement functions) provides the potential for sensitive detection of target presence (as illustrated by the simulated results) it comes at the cost of greater sensitivity to target models and potential instability during calculation of the measurement corrections.

It is somewhat surprising that the Rayleigh model performs so well. Part of its success is due to the relative flatness of the Rayleigh curve versus measured values (at least in the region below the limiting threshold) which tends to desensitize the likelihood ratio calculation.

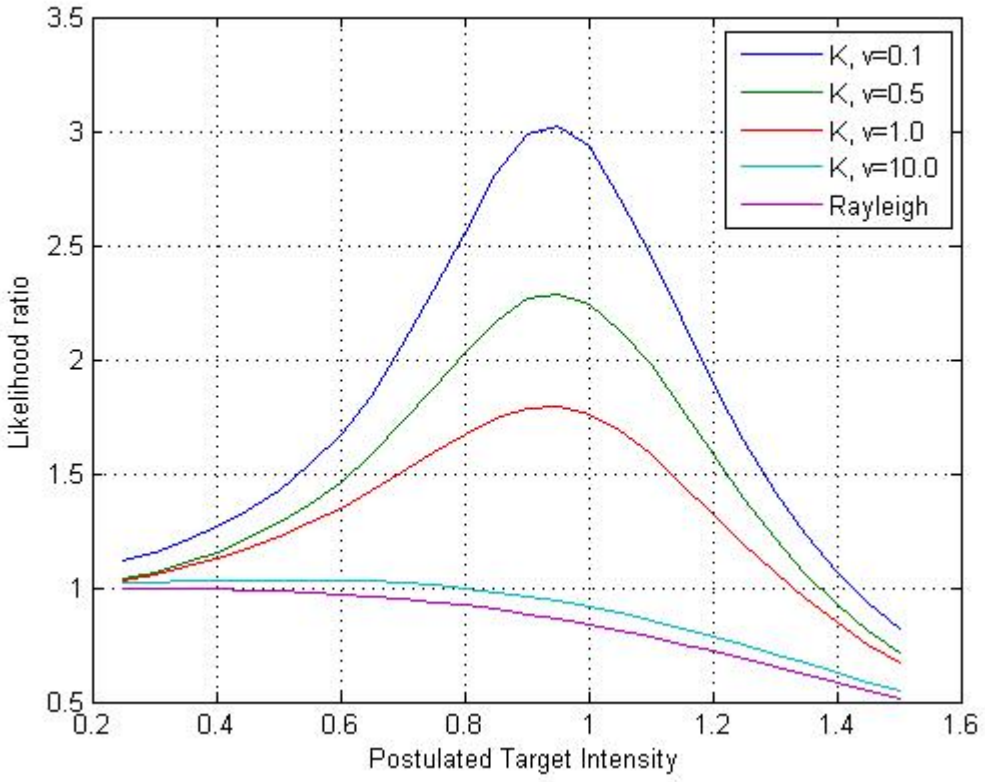

Figure 19: *Variation of likelihood ratio versus postulated signal intensity for clutter statistics assumed to follow Rayleigh pdf and K pdf for shape parameters of 0.1, 0.5, 1.0 and 10. Measured signal value is held constant at 1.0 and mean clutter power is held constant at 1.0.*

Figure 19 presents additional curves illustrating the dependence of the likelihood ratio on the choice of target intensity. It is readily apparent that the K based curves exhibit much more sharply peaked behaviour then the Rayleigh models, indicating the need to more accurately specify the target intensity. Since this value is typically not known *a priori* it represents another potentially significant cause for 'de-tuning' of the measurement correction model with respect to the data and a subsequent collapse of performance.

Another parameter requiring specification in the likelihood calculation is mean clutter power. While the examination of dependency of calculated likelihood ratios with variations of clutter power (the only parameter required for the Rayleigh clutter model) reveals significant sensitivities, it is typically much easier to obtain an accurate estimate of the mean power (first order moment) using fewer samples then it is to obtain accurate shape parameter estimates (requires higher order moments). In addition, as discussed above, the KA approach requires the additional calculation of σ_{sp} and $\bar{N}$, a difficult process with a high potential for inducing further mismatches between the postulated clutter model and the real clutter

characteristics.

It is interesting to note that both the K and KA based TkBD results demonstrated their best detection performance in a small localized portion of the surveillance area. This suggests that the model mismatches may be due to insufficient resolution of the variation of clutter parameters, such as shape parameter, with location. While this suggests a possible avenue of improvement it may be practically impossible to spatially characterize the clutter parameters more finely due to the minimum sample size requirements for parameter estimation.

This page intentionally left blank.

7 Conclusion

For the data analysed in this study, the CV models demonstrate superior performance in comparison with diffusion models for the case of a highly manoeuvrable but fast moving boat. Both Gaussian and Rayleigh sea clutter models give similar performance although initial examination of sea clutter characteristics would suggest that the Rayleigh distribution is a closer match. It is difficult to be definitive as why this apparent discrepancy occurs since neither the Guassian nor the Rayleigh is a true representation of real clutter but it is likely that one contributing factor is that the Gaussian target plus clutter model provided a better match to the fading nature of the real target returns in this study then the assumed Ricean model arising from the assumption of a Swerling 0 target in Rayleigh clutter. In addition, calculation of the measurement spread function is essentially equivalent to the application of a spatial matched filter. Therefore, the output of the matched filter for both Gaussian and Rayleigh sea clutter models will approach a Gaussian distribution per the central limit theorem. Either distribution will likely be effective for use with non-spiky clutter but the Rayleigh distribution is the preferred implementation for spiky clutter due to its straightforward extension to a compound-Gaussian distribution.

The results of the TkBD nonlinear filtering using Swerling 0, 1 and 3 target models provide some insights into the applicability of the models for the detection of small manoeuvring targets in high resolution sea clutter. The Swerling 0 model is observed to exhibit a heightened sensitivity to changes in measured signal strength, at least for the current data set. This provides enhanced detection of the maritime targets but at the cost of more strongly peaked or multi-modal posterior density. None of the Swerling models tested provides universally superior detection performance. The choice of Swerling model will likely need to be considered in conjunction with the design of any post-TkBD tracking that might be applied. The Swerling 0 model appears to be most effective when several posterior peaks are identified as potential targets or tracklets; where it is recognized that many will represent false targets. However, this approach requires that the post-TkBD tracking algorithms have the capability to reliably promote the tracklets to firm track status or terminate them. Conversely, the use of Swerling 1 or 3 target models may allow for a simplified detection and post-TkBD algorithm but at the cost of reduced detection sensitivity.

The characterization of sea clutter is complicated by the presence of infrequent but high amplitude sea clutter spikes in the data. These spikes are difficult to distinguish from real clutter; however, it was observed from the processing of simulated data sets that the potential exists for excellent detection performance via TkBD processing if the pdf presumed during the calculation of the measurement correction is closely matched to the actual clutter characteristics. In contrast, testing against real data reveals that the TkBD approaches can be highly sensitive to even small mismatches between real data and postulated pdfs that are a better fit to the amplitude distribution of the data than the Rayleigh pdf. In this report it was shown that the utilization of K and KA distributed models, which appeared to be

well matched to the real clutter, nevertheless demonstrated much reduced performance with respect to a simple Rayleigh model employing an ad hoc limitation step to de-emphasise the sea clutter spike. A major reason for this is the inability of the simple clutter models to account for the local correlation structure present in the real clutter.

References

[1] Haddad, Z. S. and Simanaca, S. R. (1995), Filtering Image Records Using Wavelets and the Zakai Equation, *IEEE Transactions on Pattern Analysis and Machine Intelligence*, 17(11), 1069–1078.

[2] Kligys, Skirmantas, Rozovsky, Boris, and Tartakovsky, Alexander (1998), Detection Algorithms And Track Before Detect Architecture Based On Nonlinear Filtering For Infrared Search And Track Systems, Technical Report Center for Applied Mathematical Sciences, University of Southern California.

[3] McDonald, Michael K., Dunne, Darcy, Damini, Anthony, and Kirubarajan, Thiagalingam (2009), Event-based characterization and simulation of sea clutter, Vol. 7445, p. 744505, SPIE.

[4] Ristic, B., Arulampalam, S., and Gordon, N. (2004), Beyond the Kalman Filter: Particle Filters for Tracking Applications, Artech House.

[5] Jazwinski, A. H. (2007), Stochastic Processes and Filtering Theory, Dover Publications.

[6] Kastella, K. and Kreucher, C. (2005), Multiple model nonlinear filtering for low signal ground target applications, *Aerospace and Electronic Systems, IEEE Transactions on*, 41(2), 549–564.

[7] Ames, W. F. (1977), Numerical Methods for Partial Differential Equations, 2nd ed, New York: Academic Press.

[8] Golub, G. H. and Loan, C. F. Van (1989), Matrix computations, 2 ed, Baltimore and London: John Hopkins University Press.

[9] Armstrong, B. C. and Griffiths, H. D. (1991), CFAR detection of fluctuating targets in spatially correlated K-distributed clutter, *IEE Proc. F, Radar, Sonar and Navigation*, 138(2), 139–152.

[10] Walker, D. (2000), Experimentally motivated model for low grazing angle radar Doppler spectra of the sea surface, *IEE Proc F, Radar Sonar Navig.*, 147(3), 114–120.

[11] Ward, K. D., Baker, C. J., and Watts, S. (1990), Maritime Surveillance Radar Part 1: Radar scattering from the ocean surface, *IEE Proc F, Radar Sonar Navig*, 137(2), 51–62.

[12] Rutten, M. G., Gordon, N., and Maskell, S. (2005), Recursive track-before-detect with target amplitude fluctuations, *IEE Proc F, Radar Sonar Navig*, 152(5), 345–352.

[13] Hou, X. and Morinaga, N. (1989), Detection Performance in K-Distributed and Correlated Rayleigh Clutters, *IEEE Transactions on Aerospace and Electronic Systems*, 25(5), 634–641.

[14] Salmond, D. J. and Birch, H. (2001), A particle filter for track-before-detect, In *Proceedings American Control Conference*, pp. 3755–3760, Arlington, VA.

[15] Meyer, D. P. and Mayer, H. A. (1973), Radar Target Detection, Academic Press.

[16] Ward, K. D. and Tough, R. J. (2002), Radar detection performance in sea clutter with discrete spikes, In *International Radar Conference*, IEE.

[17] Watts, S., Ward, K. D., and Tough, R. J. A. (2005), The Physics and modelling of discrete spikes in radar sea clutter, In *IEEE International Radar Conference*, pp. 72–77.

[18] Blacknell, D. and Tough, R. J. A. (2001), Parameter estimation for the K-distribution based on $z \log z$, *IEE Proc. F, Radar Sonar and Navigation*, 148(6), 309–312.

[19] McDonald, M. K. and Balaji, B. (2007), Continuous-Discrete Filtering for Dim Manoeuvring Maritime Targets, In *Proccedings of the Tenth International Conference on Information Fusion*, ICIF, Quebec City, QC, Canada.

[20] McDonald, M. K. and Balaji, B. (2008), Track-Before-Detect Using Swerling 0, 1 and 3 Target Models for small manoeuvring Targets, *EURASIP Journal on Advances in Signal Processing*.

DOCUMENT CONTROL DATA

(Security classification of title, body of abstract and indexing annotation must be entered when document is classified)

1. ORIGINATOR (The name and address of the organization preparing the document. Organizations for whom the document was prepared, e.g. Centre sponsoring a contractor's report, or tasking agency, are entered in section 8.)

   Defence R&D Canada – Ottawa
   3701 Carling Avenue, Ottawa, Ontario, Canada
   K1A 0Z4

2. SECURITY CLASSIFICATION (Overall security classification of the document including special warning terms if applicable.)

   UNCLASSIFIED

3. TITLE (The complete document title as indicated on the title page. Its classification should be indicated by the appropriate abbreviation (S, C or U) in parentheses after the title.)

   The application of track before detect techniques against maritime surface targets

4. AUTHORS (Last name, followed by initials – ranks, titles, etc. not to be used.)

   McDonald, M.; Balaji, B.

5. DATE OF PUBLICATION (Month and year of publication of document.)	6a. NO. OF PAGES (Total containing information. Include Annexes, Appendices, etc.)	6b. NO. OF REFS (Total cited in document.)
February 2010	60	20

7. DESCRIPTIVE NOTES (The category of the document, e.g. technical report, technical note or memorandum. If appropriate, enter the type of report, e.g. interim, progress, summary, annual or final. Give the inclusive dates when a specific reporting period is covered.)

   Technical Report

8. SPONSORING ACTIVITY (The name of the department project office or laboratory sponsoring the research and development – include address.)

   Defence R&D Canada – Ottawa
   3701 Carling Avenue, Ottawa, Ontario, Canada K1A 0Z4

9a. PROJECT NO. (The applicable research and development project number under which the document was written. Please specify whether project or grant.)	9b. GRANT OR CONTRACT NO. (If appropriate, the applicable number under which the document was written.)
13dz03	

10a. ORIGINATOR'S DOCUMENT NUMBER (The official document number by which the document is identified by the originating activity. This number must be unique to this document.)	10b. OTHER DOCUMENT NO(s). (Any other numbers which may be assigned this document either by the originator or by the sponsor.)
DRDC Ottawa TR 2009-246	

11. DOCUMENT AVAILABILITY (Any limitations on further dissemination of the document, other than those imposed by security classification.)

   (X) Unlimited distribution
   ( ) Defence departments and defence contractors; further distribution only as approved
   ( ) Defence departments and Canadian defence contractors; further distribution only as approved
   ( ) Government departments and agencies; further distribution only as approved
   ( ) Defence departments; further distribution only as approved
   ( ) Other (please specify):

12. DOCUMENT ANNOUNCEMENT (Any limitation to the bibliographic announcement of this document. This will normally correspond to the Document Availability (11). However, where further distribution (beyond the audience specified in (11)) is possible, a wider announcement audience may be selected.)

   UNLIMITED

13. ABSTRACT (A brief and factual summary of the document. It may also appear elsewhere in the body of the document itself. It is highly desirable that the abstract of classified documents be unclassified. Each paragraph of the abstract shall begin with an indication of the security classification of the information in the paragraph (unless the document itself is unclassified) represented as (S), (C), (R), or (U). It is not necessary to include here abstracts in both official languages unless the text is bilingual.)

Real radar data containing a small manoeuvring boat in sea clutter was processed using a grid based finite difference implementation of continuous-discrete filtering. An examination was undertaken to determine the appropriate dynamic, target amplitude and clutter amplitude models which should be utilized to allow the successful application of Track Before Detect techniques (TkBD). Both two dimensional diffusion and four dimensional constant velocity models were implemented using Gaussian and Rayleigh sea clutter models. Superior performance was observed for the constant velocity model and significant sensitivity was noted due to mismatches between actual clutter characteristics and Gaussian and Rayleigh models. TkBD performance was examined assuming a Rayleigh sea clutter model with embedded Swerling 0, 1 or 3 target signal models. The Swerling 0 model was observed to exhibit a heightened sensitivity to changes in measured signal strength and provided improved detection of the maritime target examined in comparison with Swerling 1 and 3 targets at the cost of more peaked or multi-modal posterior density. The potential for achieving significant detection performance improvements by utilizing K and KA distributed clutter models in place of the simpler Rayleigh distribution was demonstrated through analysis of simulated data representing spiky sea clutter. However, additional analysis using real data revealed that use of a probability distribution function more closely matched to the observed real sea clutter returns does not necessarily result in improved performance. For the data set examined, significantly degraded performance was observed when K and KA based processing is used in place of a Rayleigh based processor utilizing a simple likelihood limiting step to compensate for model mismatches due to sea clutter spikes.

14. KEYWORDS, DESCRIPTORS or IDENTIFIERS (Technically meaningful terms or short phrases that characterize a document and could be helpful in cataloguing the document. They should be selected so that no security classification is required. Identifiers, such as equipment model designation, trade name, military project code name, geographic location may also be included. If possible keywords should be selected from a published thesaurus. e.g. Thesaurus of Engineering and Scientific Terms (TEST) and that thesaurus identified. If it is not possible to select indexing terms which are Unclassified, the classification of each should be indicated as with the title.)

Nonlinear Filter
Maritime Radar Surveillance
Tracking

Defence R&D Canada

Canada's leader in Defence
and National Security
Science and Technology

R & D pour la défense Canada

Chef de file au Canada en matière
de science et de technologie pour
la défense et la sécurité nationale

www.drdc-rddc.gc.ca